

POLITECNICO DI TORINO

**A STUDY OF QUANTUM
ISOTOPIC SIEVING
THROUGH CARBON
NANOTUBES**

by

Devagnik Dasgupta

A thesis submitted in partial fulfillment for the
degree of Doctor of Philosophy

in the

Department of Mathematical Sciences

February 2013

POLITECNICO DI TORINO

Abstract

Department of Mathematical Sciences

Doctor of Philosophy

by [Devagnik Dasgupta](#)

The theory of molecular sieving has long been a subject of importance because of its widespread technological applications. Classical molecular sieving mainly depends on the size and shape of the guest molecules and the size of the host solid. However, isotope separation is usually very difficult to achieve through classical sieving, as the isotopes generally have the same shape and size and differ only in mass. One way to resolve such an issue is through the applications of quantum effects which are prominent inside nanotubes and nanopores of diameters that are comparable with the De-broglie wavelength λ of the molecules.

In the recent past, various authors have calculated the selectivity of isotopes (mainly hydrogen-deuterium) diffusing through nanotubes where they predict the preferable selectivity of the heavier species over the lighter species based on the difference in their zero point energies. The effects are more pronounced at low temperature regimes where quantum effects are dominant. However, this kind of sieving, though showing appreciable preference to the heavier isotope, is far from being "perfect" and also technologically expensive as very low temperature range is required.

In our work, we try to search for a technologically inexpensive method for realising isotope sieving by introducing two nanotubes of different radii that are coupled together. Through a mathematical model that best describes the situation, we try to search for a "perfect" sieving of the hydrogen-deuterium isotopes over a wide temperature range, not restricting ourselves to very low temperatures. As we have found out and will be described in the following work, the two nanotube system does indeed go a long way towards a technologically efficient way of realising "perfect" sieving. We also employ MD simulations to investigate kinetic sieving of isotopes through nanotubes. The quantum effects are introduced into the system via a modified FH potential, and ring polymer MD simulation is used to model the system. Though the selectivity values we found in our results are lower in comparison to those already predicted using equilibrium sieving, our results show similar qualitative behaviour to the same approach adopted by others previously using different sieving material.

Acknowledgements

It would not have been possible to write this doctoral thesis without the help and support of the kind people around me, to only some of whom it is possible to give particular mention here.

The first name that comes to my mind is of course of my principal supervisor, Prof. Lamberto Rondoni, who has been a constant source of inspiration throughout the three long years that I have known him, and whose help, support and patience has made this thesis possible, not to mention the invaluable inputs that he has provided towards the development of my research. I am also extremely thankful to Prof. Owen Jepps for the fruitful discussions we have had over the years.

I would like to acknowledge the financial support provided towards the development of this thesis by the Italian Institute of Technology (IIT), who funded my research, and for providing me with an office as well as other necessary facilities.

I am extremely grateful to Dr. Stefano Bernardi and Prof. Debra Bernhardt of AIBN, University of Queensland, who I was fortunate enough to work with and who were gracious enough to host me in Australia. A big thanks especially to Stefano who has made a valuable contribution towards this thesis, and whose friendship I cherish dearly.

I would also like to thank all the teachers and professors throughout my school and university who have inspired me to be a student of science. A big nod of acknowledgement to all my friends, who have been with me every step of the way. And last, but certainly not the least, a word about my wonderful family, without whom I would have been nothing that I am today. My parents and my little sister have given me their unequivocal support throughout, as always, for which my mere expression of thanks likewise does not suffice.

Contents

Abstract	ii
Acknowledgements	iii
List of Figures	vi
List of Tables	vii
Physical Constants	viii
Symbols	ix
1 INTRODUCTION	2
1.1 What is molecular sieving?	2
1.2 Why quantum?	2
1.3 Literature Review	3
1.4 Our Aim	18
2 THEORETICAL TOOLS	20
2.1 A brief discussion about carbon nanotube structures	20
2.2 Energy eigenvalues for a particle in a square circular potential	23
2.2.1 Quantum Solutions	24
2.2.2 Classical probability distribution for position	26
2.3 Bessel functions:Introduction,few properties and recurrence relation	27
2.3.1 Bessel functions of the first and second kind	28
2.3.2 Modified Bessel functions	32
2.3.3 Recurrence relations	33
2.4 Maxwell-Boltzmann Distribution	35
2.4.1 Distribution for the momentum vector	35
2.4.2 Distribution for velocity	36
3 THEORETICAL MODEL	38
3.1 From reservoir to nanochannel	39

3.2	Quantized energy levels in the nanochannels	43
4	RESULTS	47
4.1	Calculation of energy levels	47
4.2	Inside the first nanochannel	48
4.3	Inside the second channel	50
4.4	A general theorem on correspondence	54
4.5	Comparison between percentage of H_2 and D_2 in the second channel	56
4.6	Distribution of nanotubes	57
4.6.1	Distribution of nanotubes in the second channel	59
5	KINETIC SIEVING OF ISOTOPES	63
5.1	Theoretical Outline	63
5.2	Results	65
6	CONCLUSION	71

List of Figures

2.1	carbon nanotubes	22
2.2	bessel function of first kind	31
2.3	bessel function of second kind	32
2.4	modified bessel function of first kind	32
2.5	modified bessel function of second kind	34
2.6	Maxwell-Boltzmann energy distribution for two different temperatures	37
3.1	schematic diagram 1	39
3.2	schematic diagram 2	41
3.3	schematic diagram 3	45
4.1	dN/N vs temperature(in Celsius)for ground state energy($m = 0$) . .	49
4.2	comparison between percentages at 100K	52
4.3	comparison between percentages at 200K	53
4.4	comparison between percentages at 300K	54
4.5	coincidence of zeroes of bessel function when $a=5b$	55
4.6	comparison of percentages of isotopes present inside the first nanotube for uniform distribution	59
4.7	comparison of percentages of isotopes present inside the second nanotube for normal distribution	60
4.8	comparison of percentage of hydrogen inside second nanotube for different distributions	62
4.9	comparison of percentage of deuterium inside second nanotube for different distributions	62
5.1	A physical representation of the simulation setup	64
5.2	sample run of a single simulation(this one is for a (6,6) nanotube at 40 K)	66
5.3	selectivity vs T curve for a (2,8) nanotube	66
5.4	selectivity vs T curve for a (6,6) nanotube	67
5.5	selectivity vs T curve for a (8,8) nanotube	67
5.6	selectivity vs T curve for a (10,10) nanotube	68
5.7	change in molar concentration of the isotopes inside the two reservoirs for a typical simulation(this one is for a (6,6) nanotube at 40K)	69
5.8	comparison of selectivity for different nanotubes	69

List of Tables

2.1	Structural parameters of armchair (<i>A</i>), zigzag (<i>Z</i>) and chiral (<i>C</i>) nanotubes	23
4.1	energy levels (in K) for hydrogen for various <i>m</i> values	48
4.2	energy levels (in K) for deuterium for various <i>m</i> values	48
4.3	percentage of hydrogen(in units of 10^{-3}) inside first nanotube for various <i>m</i> values	49
4.4	percentage of hydrogen(in units of 10^{-3}) inside first nanotube for various temperature (<i>m</i> is fixed at 0)	49
4.5	percentage of deuterium(in units of 10^{-3}) inside first nanotube for various temperature (<i>m</i> is fixed at 0)	50
4.6	First few energy levels of hydrogen(in <i>K</i>) inside second nanotube for varying tube radii (<i>m</i> is fixed at 0)	51
4.7	First few energy levels of deuterium(in <i>K</i>) inside second nanotube for varying tube radii (<i>m</i> is fixed at 0)	52
4.8	Cutoff for Maxwell-Boltzmann distribution at various temperatures	56
4.9	Percentage of molecules (in units of 10^{-3}) allowed into the second channel	57
4.10	Percentage of molecules (in units of 10^{-3}) absorbed inside nanotubes with varying width at room temperature with $d\omega = 1$	58
4.11	Percentage of molecules (in units of 10^{-3}) absorbed inside nanotubes with varying width at room temperature with $d\omega = 1$	59
4.12	Percentage of molecules (in units of 10^{-3}) absorbed inside nanotubes with varying temperatures considering uniform distribution	61
4.13	Percentage of molecules (in units of 10^{-3}) absorbed inside nanotubes with varying temperatures considering gaussian distribution	61

Physical Constants

$$\text{Boltzmann constant } k_b = 1.380\,648 \times 10^{23} \text{ JK}^{-1}$$

$$\text{Planck's constant } \hbar = 1.054\,571 \times 10^{-34} \text{ Js}$$

Symbols

r	radius
$U(r)$	classical pair potential
m	angular momentum quantum number
λ	De-Broglie wavelength
μ	mass of molecule
ψ	wave-function
θ	angle
ϵ	depth of potential well(L-J parameter)
σ	finite distance at which the inter particle potential is zero(L-J parameter)

*To my beloved East Bengal FC, the best football club in
the world. Joy EB! ...*

1

Chapter 1

INTRODUCTION

1.1 What is molecular sieving?

Molecular sieving is normally defined as the process that is used to separate two molecules from a mixture. Classically, a pore or an opening is used as a sieve (hence the name sieving) which allows the molecule with the smaller size to pass through and refuses to let the bigger one pass. However, as simple as it sounds, this process is futile when used to separate isotopes as normally isotopes of a same species are almost similar in size and shape, differing only in mass.

1.2 Why quantum?

In the nano regime, the diameter of the nanotube or nanopore is comparable in size to the De-broglie wavelength of the molecule. The quantum effects thus become prominent due to constriction in size available for the movement of molecules.

1.3 Literature Review

The concept of quantum sieving was introduced by Beenakker *et al*[1] through a simplistic model. The authors considered the nanoporous materials of diameter d such that $d \approx \lambda$ (where $\lambda=h/mv_r$ is the de-broglie wavelength associated with the molecule). This resulted in the quantization of transverse motion of the particles and an overall reduced dimensionality of the particle ensemble. The authors limited their discussions to low molecular densities in the pores such that the molecule-molecule interaction was negligible to the molecule-wall interaction. The pores were considered to be cylindrical with a constant diameter, and the motion of the molecules could be separated into two independent components, radial and axial. While along the axial direction, the motion was free i.e classical, along the radial direction the energies were quantized as the particles moved in a square circular potential well of depth ϵ which arises due to the interaction between the molecules and the walls of the nanotube. The quantized energy levels were given as

$$E_i = \epsilon + \frac{2\gamma_i^2 \hbar^2}{(d - \sigma)^2 m} \quad (1.1)$$

where γ_i are related to zeroes of the bessel functions and σ is the molecular diameter.

It can be seen directly from the expression for energy that E_i is inversely proportional to mass, which indicates lighter particles have a higher quantization and vice versa. This very fact is exploited explicitly in our studies. The authors concluded that quantum effects were characterized by two main parameters-

i) E_0/ϵ , the relative importance of the ground state energy with respect to the potential energy originating from molecule wall interactions.

ii) $(E_1 - E_0)/k_b T$, the excitation energy of the first excited level compared to the thermal energy of the molecule.

If $E_0/\epsilon > 1$, this implies that a molecule entering the channel from a free space encounters an energy barrier that can only be overcome by thermal excitation. Physically, it means that zero point motion overcompensates the attractive molecule-wall interaction and will result in a decrease of the molecular density inside the nanochannel. They termed this effect, where the adsorption in porous media is dominated by the zero point energy, as *quantum sieving*. The authors also gave some estimates about the viability of quantum sieving in various molecules. For example, for Helium isotopes, they concluded that the situation $E_0/\epsilon > 1$ will be realised for diameters of about 0.4 nm.

The second quantum effect arose from the increase in level splitting with decreasing d and m . $(E_1 - E_0)/k_bT \gg 1$, indicates that the level splitting in the well becomes so large that all particles for the radial motion are exclusively in their ground state leaving the first excited state vacant. Thus the system behaves like a 1D gas, in which two degrees of freedom are frozen and only the axial translational motion remains. This situation, according to the authors, should be realized for $T \leq 78$ K for hydrogen and helium molecules. They also concluded that since isotopes will have the same values of σ and ϵ , the adsorption through the channels would be dominated by the respective E_0 values, and in turn, their masses. This also implied that the heavier isotope should be favourably adsorbed in preference to the lighter one.

This basic idea was later expanded upon by several authors using realistic description of molecules and microporous adsorbents, notably by Johnson and co-workers [2, 3]. Using a simple theoretical model and extensive path integral calculations, the authors showed that molecular tritium will be readily adsorbed in micropores whereas molecular hydrogen will be excluded as a result of quantum sieving. They predicted that interstitial channels of close packed carbon nanotube bundles or ropes have the correct pore size and solid-fluid potential to effectively sieve

mixtures of H_2 and T_2 . The theoretical model was based on considering a gas mixture (H_2 and T_2) in equilibrium with the adsorbed phase. Like the previous authors, the gas mixture was considered to be of sufficiently low density so that the adsorbate formed a classical 1D gas, with unhindered motion along the axis and quantized radial degrees of freedom in their ground state. However, an important point to remember is that this treatment is only valid for very low temperatures. In this model, the ground state energy of species i 's transverse wave function is denoted by E_i . The chemical potential of this adsorbed component is given by Stan *et al*[4, 5],

$$\mu_i^{ads} = E_i + k_b T \ln\left(\frac{\rho_i \lambda_i}{q_i}\right) \quad (1.2)$$

where

ρ_i =number density of component i in the pore

$\lambda_i = \sqrt{2\pi\hbar^2/\mu_i k_b T}$ is the de-broglie thermal wavelength

q_i =internal molecular partition function

μ_i =mass of the component i

T =absolute temperature

Assuming that the bulk phase is an ideal gas (following Maxwell-Boltzmann law of distribution) at very low pressure, the chemical potential of the same component μ_i^{bulk} is given as,

$$\mu_i^{bulk} = k_b T \ln\left(\frac{n_i \lambda_i^3}{q_i}\right) \quad (1.3)$$

where n_i is the bulk phase density of the component i

The adsorbed phase is in equilibrium with the bulk phase, so $\mu_i^{ads} = \mu_i^{bulk}$. Thus assuming q_i is the same in adsorbed and bulk phase,

$$\rho_i = n_i \lambda_i^2 e^{-E_i/k_b T} \quad (1.4)$$

if the coadsorption of two distinct components are now considered, the selectivity of component i over j is defined as

$$S = \frac{x_i/x_j}{y_i/y_j} \quad (1.5)$$

where x and y refer to the mole fractions in the adsorbed and bulk phase respectively. The analysis above yields the selectivity in the limit of low pressure and temperature denoted by S_0 . Combining eqns(1.4) and (1.5)

$$S_0 = \left(\frac{\mu_j}{\mu_i}\right) \exp\left[-\frac{E_i - E_j}{k_b T}\right] \quad (1.6)$$

It is noted that S_0 is independent of the bulk phase composition. A simple example as demonstrated by the authors elucidates the significance of this relation. A case where the adsorption potential is radially symmetric harmonic potential is considered i.e $V(r)=Kr^2/2$. Then, the ground state energy of the species μ_i is given by $\frac{\hbar}{2}\sqrt{\frac{K}{\mu_i}}$. Since the two isotopes of the adsorbed species with mass μ_1 and μ_2 are subject to the same potential, the low pressure selectivity of component 2 over component 1 is given by

$$S_0 = \frac{\mu_1}{\mu_2} \exp\left[-\frac{\hbar\sqrt{K}}{k_b T} \left(\frac{1}{\sqrt{\mu_2}} - \frac{1}{\sqrt{\mu_1}}\right)\right] \quad (1.7)$$

thus if $\mu_1 < \mu_2$, then $S_0 > 1$ at low temperatures. This shows that the pore selectively adsorbs the heavier isotope over the lighter one. Although the simple form of harmonic potential for zero point energy of isotopes is highly exaggerated, yet the preference of heavy over light isotope is a generic feature of quantum sieving. Eqn (1.7) is valid when the quantum confinement of the adsorbate is two dimensional. In very large pores, for species that adsorb close to pore wall, quantum confinement will occur radially but not angularly. In this case of one dimensional

confinement, S_0 is given by

$$S_0 = \sqrt{\frac{\mu_j}{\mu_i}} \exp\left[-\frac{E_i - E_j}{k_b T}\right] \quad (1.8)$$

where E_i is the ground state energy due to the quantization in the direction normal to pore wall.

This theory was extended by the authors by relaxing the assumption that at low temperatures only ground states are populated. If E^l is the l^{th} energy level for the quantized transverse motion, the chemical potential for the adsorbed component is given by

$$\mu_i^{ads} = -k_b T \ln\left(\sum_l e^{-E_i^l/k_b T}\right) + k_b T \ln\left(\frac{\rho_i \lambda_i}{q_i}\right) \quad (1.9)$$

which reduces to eqn (1.2) when only the ground state is populated. Considering the population of excited states, eqn (1.9) in combination with eqn (1.3) gives the selectivity as

$$S_0 = \frac{\mu_j}{\mu_i} \left[\frac{\sum_l \exp(-E_i^l/k_b T)}{\sum_l \exp(-E_j^l/k_b T)} \right] \quad (1.10)$$

To ensure the validity of the theoretical model, calculations were extended to the numerical domain by almost accurate representation of adsorbate potential with atom-atom potential functions (like Lennard-Jones potential). For the evaluation of S_0 , *path integral Monte Carlo* (PIMC) methods were used with a final expression for S_0 given as

$$S_0 = \frac{\int d\Gamma_1 \int d\omega_1 \int_0^R r dr \exp[-U_1/k_b T]}{\int d\Gamma_1 \int d\omega_1 \int_0^R r dr \exp[-U_2/k_b T]} \quad (1.11)$$

where

U = the configurational energy

Γ, ω = path's internal conformation and orientation

r = the radial position of the ring's center of mass

R = tube's radius

For effective quantum sieving, the authors found that fullerene single wall carbon nanotubes (SWNT) are excellent candidates as the pore widths of these tubes are slightly larger than the molecular diameter of adsorbate molecules. They calculated the zero pressure selectivity S_0 for SWNTs of various diameters. The solid fluid potential was generated for various (n, m) tubes (nomenclature as used by Hamada *et al* [6]) by using the Crowell-Brown [7] potential for hydrogen-carbon interactions. They found that SWNTs wider than $d \approx 7\text{\AA}$ exhibited weak selectivity while those smaller were predicted to show dramatically large selectivities. The authors inferred that this is because below 7\AA , the adsorbed molecules are highly confined and hence possess significant zero point energies whereas as the tube diameter goes beyond 7\AA , molecules preferentially adsorb near the pore walls rather than the pore center, leading to the type of 1D confinement given by eqn(1.8). A plot of $S_0(T_2/H_2)$ at 20 K for SWNTs of various sizes shows that selectivity increases as tube diameter decreases, reaching a value of almost 10^5 for a (3,6) tube [2, 3]. Furthermore, the agreement between eqn(1.6) and the path integral simulations were found to be excellent. One interesting feature as noted by the authors were that the lowest selectivity occurs at the transition between 2D and 1D confinement, as in the (6,6) nanotube. The reason given was that the interaction potential inside the (6,6) nanotube being flatter and broader at the well as compared to either narrower or wider tubes, the adsorbate wave functions were more delocalized, making them an unlikely candidate for confinement of small molecules.

Another important feature noted in the same papers were that quantum sieving could be effectively achieved by allowing adsorption in the interstitial regions formed by ordered bundles of SWNTs. Stan *et al*[5] performed theoretical calculations showing that *He* and *Ne* can be strongly physisorbed inside these interstices. This is beneficial because the interstices of a nanotube bundle can have widths which are lesser than low diameter nanotubes, that are difficult to synthesize. As shown in [3], the selectivity in the interstice of a (10,10) nanotube is

comparable to the highest selectivities observed in the smallest *SWNTs*. Apart from the T_2 - H_2 system (which gives the best results because of highest mass difference), several other systems like HD - H_2 , CH_4 - CD_4 and He^3 - He^4 were considered which all showed the general preference of the heavier specimen getting selectively adsorbed in preference to the lighter one. The authors also calculated the selectivity for different temperatures and found that it drops dramatically as temperature is increased. For example at 77K, the selectivity of T_2 over H_2 is about 5.2, which is only about 0.05% of the corresponding value at 20K. This led them to conclude that quantum sieving is strongly temperature dependent and is a general property of adsorption of isotopic mixtures.

The model proposed by the previous authors treated the molecules as spherical objects with isotropic rotations when confined and neglected the small effects that arise from the asymmetry of the molecules. Hathorn *et al*[8] sought to correct this issue and proposed that in addition to radial confinement, the hindered molecular rotation in carbon nanotubes should contribute to quantum sieving. The rotational energy of the diatomic molecules was given as $E = J(J + 1)$ where J is the total angular momentum. E might be zero when J is zero. Just as in the previous model, the translational motion was quantized, in the new model the authors considered the quantization of rotational motion.

To proceed towards the eventual quantization, the partition function Q was considered initially. In case of non-interacting degrees of freedom, the partition function reduced to a product of independent partition functions over the different degrees of freedom.

$$Q = Q_{trans}Q_{rot} \quad (1.12)$$

Considering a mixture of noninteracting species of molecules, the ratio of concentration of adsorbed molecules to those in gas phase is given by S (the authors term this as the separation factor, which is similar to the selectivity used in the previous

example). An explicit expression is given as

$$S = \left(\frac{Q_{ads,1}}{Q_{ads,2}} \right) \left(\frac{Q_{free,1}}{Q_{free,2}} \right) \quad (1.13)$$

The authors note that the approximation that the rotational and translational motions can always be decoupled inside carbon nanotubes is not exact. As an example, when the translational motion of the molecules takes place near the wall, the rotational potential will be higher, and the cylindrical symmetry will be lost. In the model they discuss, the authors consider that the molecule is in the center of the nanotube corresponding to average translational motion. This results in minimum perturbation of rotational eigenvalues as the molecule is in the maximum possible distance away from the walls. For the calculation of the partition function of hindered rotational motion, the eigenvalues of the restricted rotor were used. In their model, the authors considered a linear rigid rotor whose classical mechanical hamiltonian was given as

$$H = B \left(p_\theta^2 + \frac{p_\phi^2}{\sin^2 \theta} \right) + V(\theta, \phi) \quad (1.14)$$

where the first term represents the rotational kinetic energy in polar coordinates and the second term indicates the potential interaction between the molecule and the environment. The constant, $B = \hbar/2\mu d^2$ is the rotational constant of the diatomic molecule, with a bond length d and a reduced mass μ . The quantum partition function is given by

$$Q = \sum_i \exp(-\beta E_i) \quad (1.15)$$

where i stands for the quantum levels of the system, each with energy E_i . The free quantum -rotational partition function is given as

$$Q_{rot,free} = \sum_i g(J)(2J + 1) \exp[-\beta B(J)(J + 1)] \quad (1.16)$$

where $g(J)$ is the weight factor due to nuclear spin statistics. For homonuclear diatomics with half-integral spin (i.e H_2 and T_2 , both with nuclear spin $1/2$),

$$Q_{rot,free} = \sum_{J_{even}} (2J + 1) \exp[-\beta B(J)(J + 1)] + 3 \sum_{J_{odd}} (2J + 1) \exp[-\beta B(J)(J + 1)] \quad (1.17)$$

For D_2 isotope with integral spin 1, the partition function is given by

$$Q_{rot,free} = 6 \sum_{J_{even}} (2J + 1) \exp[-\beta B(J)(J + 1)] + 3 \sum_{J_{odd}} (2J + 1) \exp[-\beta B(J)(J + 1)] \quad (1.18)$$

To calculate the quantum levels of the restricted rotor case, the authors make use of the semiclassical treatment, yielding the quantization condition

$$\oint pdq = 2\pi\hbar J(J + 1) \quad (1.19)$$

Calculation of the free rotor quantum levels with the quantization condition (eqn 1.19) lead to the exact quantum levels of the rigid rotor. For their case, the authors defined the azimuthal angle θ to be the rotation away from the principal axis of the nanotube cylinder, which was assumed to have cylindrically symmetric potential i.e $V(\theta, \phi)$ was independent of ϕ . They employed a modified Lennard-jones type potential for approximating the interaction of the molecules with the nanotube

$$V(\theta, \phi) = -2\epsilon \left(\frac{r^*}{r_{LJ}} \right)^6 + \epsilon \left(\frac{r^*}{r_{LJ}} \right)^{12} \quad (1.20)$$

with lennard Jones interaction distance between the end of the molecule and the wall of the nanotube being given by

$$r_{LJ} = R - \left(\frac{d}{2}\right) \sin\theta \quad (1.21)$$

Upon calculation of the isotopic separation due to quantization of rotational motion, the authors found that separation factors for all possible hydrogen isotopomers relative to the H_2 standard yielded a high number (up to fifteen orders of magnitude) for low temperatures ($\approx 20K$). Like the previous study, they observed that with reduced tube size and reduced temperature, the separation increased significantly. In the range of 6-8 Å cylinder diameter, they found comparable selectivity to those made in [2, 3], leading them to conclude that both translational and rotational confinement lead to significant selectivity. Furthermore, it was their opinion that combination of the two separation factors should produce larger effects than either one by itself.

Lu, Goldfield and Gray sought to explore the idea of including both rotational and translational degrees of freedom and their coupling while studying quantum sieving. In their paper [9], they study the effects of confinement in small single walled carbon nanotubes on molecular hydrogen and its isotopes. Except for the motion along nanotube axis, all other motions of the hydrogen relative to the tube were treated explicitly viz. the motion of the H_2 center-of-mass in a plane perpendicular to the tube axis and rotation about that center-of-mass. Hence the problem reduces to a four degree of freedom problem (two for translations and two for rotations). Further considering a fixed position of the molecular center of mass at the tube center, a fixed bond length of the diatomic in its equilibrium position and neglecting the motions of atoms in the carbon nanotubes, the four degrees of freedom hamiltonian is given by

$$H = \frac{-\hbar^2}{2M} \left(\frac{\partial^2}{\partial x^2} + \frac{\partial^2}{\partial y^2} \right) - B \left(\frac{1}{\sin\theta} \frac{\partial}{\partial \theta} (\sin\theta) + \frac{1}{\sin^2\theta} \frac{\partial^2}{\partial \phi^2} \right) + V(x, y, \theta, \phi) \quad (1.22)$$

where

M is the total mass of the diatomic molecule

$B = \hbar/2\mu r_e^2$ is the rotational constant

μ is the reduced mass of the molecule

r_e is the equilibrium bond length

The potential term includes all possible interactions between the atoms of the diatomic and the carbon atoms of the nanotube. The wave function, expanded in a set of real eigenfunctions of the rotational part of the Hamiltonian, is given as

$$\Psi(x, y, \theta, \phi) = \sum_{j=0}^{j_{max}} \sum_{m=0}^{m=j} P_j^m(\cos \theta) (C_j^m(x, y) \cos m\phi + D_j^m(x, y) \sin m\phi) \quad (1.23)$$

where

P_j^m is a normalized associated Legendre function

C_j^m, D_j^m are expansion coefficients

The authors used the Tersoff-Brenner potential to model the short range interactions between the H atoms and the carbons in the nanotubes whereas the long distance van der Waals forces between each hydrogen and each carbon atom were computed using L-J potential. However, their results for quantum selectivity at 20K for smaller *CNTs* were considerably smaller than those for Johnson and co-workers. They attributed this disparity to the fact that Johnson and co-workers used a different potential viz. Crowell-Brown potential which appears to be less flat for smaller nanotubes. Their calculations indicated that temperature *less* than 20 K are required to observe significant quantum effects, but modest effects might be seen at higher temperatures. They found that magnitude of quantum sieving is primarily a function of diameter, but it is not a monotonic function. The largest effects were seen in smallest nanotubes, where the molecule has 2D confinement in the center of the nanotube. *This result is perfectly in tandem with those observed*

in previous studies by different authors. They also found that lowest selectivity occurs for the (2, 8) nanotube, which is near the transition between 1D and 2D confinement and agrees with the findings of Johnson and co-workers. According to the authors, this phenomenon occurs due to the decrease in steepness of the nanotube potential as the diameter is decreased. Additionally, they inferred that strong quantum effects could also be observed in the interstitial channels of bundles of larger nanotubes, which was suggested earlier by Johnson and co-workers and Trasca *et al*[10].

In a later article[11] by the same authors, they identified three different types of confinements: one dimensional(1D), two dimensional (2D) and what they called the *extreme two dimensional(X2 - D)* confinement. The last effect arises when the nanotube radius becomes smaller than than r_e (r_e is the value of r at the minimum of H-C interactions viz. for L-J potential, $r_e=2^{1/6}\sigma$). In this case the molecules are very strongly confined to the center of the nanotube, preferentially aligned along the nanotube axis. The characteristics of the X2-D state according to the authors were steep potentials, very large ZPEs, large quantum selectivities and highly hindered rotation. One further distinguishing characteristic of the X2-D also were the small number of bound states, that is, those states that are lower in energy than a hydrogen molecule an infinite distance away from the nanotube, which is taken to be the zero of energy.

For their new work, the authors used three separate H-C interactions and compared the findings for each of them. The potentials were designated as NW, FB and WS77. The first two were L-J 6-12 interaction potentials given by

$$V(r) = 4\epsilon \left(\frac{\sigma^{12}}{r^{12}} - \frac{\sigma^6}{r^6} \right) \quad (1.24)$$

For the NW potential, $\epsilon = 18cm^{-1}$ and $\sigma = 2.78\text{\AA}$ whereas for the FB potential $\epsilon = 19.2cm^{-1}$ and $\sigma = 3.08\text{\AA}$. The WS77 potential, given by a Buckingham

form[12] is written as

$$V = Be^{-Cr} - \frac{A}{r^6} \quad (1.25)$$

with $A = 5.94eV\text{\AA}^6$, $B = 678.2eV$, and $C = 3.67\text{\AA}^{-1}$. A calculation of the well depth for various nanotubes by the authors revealed that in the NW interactions, the largest well depth occurs for the smallest nanotube which is (3, 6). However, the situation is different for the other two potentials where (2, 8) nanotube has the largest well depth.

The authors found that FB and WS77 potentials exhibit the X2-D type confinement for the (3, 6) and (8, 0) nanotubes, which however is not displayed by the NW potential. As a result, it also has considerably smaller selectivity coefficient when compared to the other two. According to the authors, this is consistent with the fact that NW potential has a smaller r_e than the other two potentials, which implies a weaker 2-D confinement. They also noted that quantum sieving and ZPE simply does not decrease with the increase of CNT radius but rather displays a minimum. The minimum corresponds to a transition from 2-D to 1-D confinement and corresponds to the smallest nanotube radius that displays 1-D confinement. By using the more realistic WS77 potential, the authors found that the results for quantum sieving were also in better agreement with those of Johnson and co-workers and in good agreement with Garberoglio *et al*[13].

Kumar and Bhatia[14] tried to examine the quantum effects on the dynamical properties of confined systems, moving on from the equilibrium properties treated in detail in the previous examples. Their simulations were done on zeolite rho, rather than carbon nanotubes. The authors used equilibrium molecular dynamics (EMD) simulation with Feynman-Hibbs (FH) modified interaction potential-

$$U_{FH}(r) = \left(\frac{6\mu}{\pi\beta\hbar^2}\right)^{\frac{3}{2}} \int d\mathbf{R} U(|\mathbf{R} + \mathbf{r}|) \exp(-6\mu R^2/\beta\hbar^2) \quad (1.26)$$

where $U(r)$ is the classical pair potential. The above expression considers the

quantum pair as having a gaussian spread of $\sqrt{\beta\hbar^2/12\mu}$ in separation where μ is the reduced mass and $\beta = 1/k_B T$.

In their EMD simulations for hydrogen isotopes in zeolite rho model, the authors used the L-J potential to represent the sorbate and host atom atom interactions. For the $H_2 - H_2$ and $D_2 - D_2$ interaction, the parameters used were $\sigma_f = 0.292nm$ and $\epsilon_f/k_b = 38K$ while for the $O - H_2$ or $O - D_2$ interaction, the parameters used were $\sigma_f = 0.273nm$ and $\epsilon_f/k_b = 76.76K$. The simulations employed by the authors solved the sytem of first order differential equations $\dot{q}_i = P_i/m$ and $\dot{P}_i = F_i - \lambda P_i$ where λ is the thermostat factor determined by the gaussian principle of least constraint, q_i and P_i are the position and momentum vectors respectively, and F_i is the net force acting on the particle.

While determining the effective potential considering quantum effects, eqn(1.26) was replaced by

$$U_{FH}(r) = U(r) + \frac{\beta\hbar^2}{24\mu} \left(U''(r) + 2\frac{U'}{r} \right) + \frac{\beta^2\hbar^4}{1152\mu^2} \left(15\frac{U'(r)}{r^3} + 4\frac{U'''(r)}{r} + U''''(r) \right) \quad (1.27)$$

The above equation was used by for both fluid-fluid as well as solid-fluid interactions. The simulation of transport in zeolite-rho by the authors showed that the quantum effects led to significant reduction in the diffusivity of the confined H_2 and D_2 , with the quantum diffusivity of the former decreasing more strongly with temperature when compared with the classical case. In the bulk fluid, the opposite effect i.e an increase of quantum diffusivity over classical one is observed and is normally attributed to quantum tunneling, where a decrease of the intermolecular potential well depth reduces the translational energy barrier. However, in case of a confined quantum fluid, despite a similar well reduction, the authors observed a reduction in diffusivity as well which they termed as *paradoxical*. The effect was observed for both the isotopes, but being stronger for H_2 consistent with its smaller mass. The primary cause for the change in diffusivity, according to the authors, was the steric hindrance caused by the swelling of the effective size parameter of

the fluid-solid interactions. One remarkable feature regarding the diffusivity of the isotopes that the authors observed was that below 150K, the heavier D_2 diffused faster. This, according to them, happens because the quantum shift in potential is smaller for D_2 compared to H_2 , and thus having the heavier mass, swelling of D_2 is smaller which ultimately leads to an increase in kinetic selectivity for D_2 with reduction in temperature. Infact, they found a dramatic increase in the quantum selectivity below 70K, with a peak value of 21.70 at about 65 K. They also commented that with the low temperature kinetic selectivity enhancement for D_2 , one could anticipate a relative increase in size for H_2 , and decrease in its well depth, leading to an increased equilibrium selectivity of D_2 . This was in agreement with what was observed in all the previous works.

In a subsequent publication [15] by the same authors, these claims were experimentally verified by neutron scattering experiments. For the simulation part, L-J potential was again used to model the fluid-fluid and fluid-zeolite interactions but with best fitted parameters of $\sigma_{H_2-H_2} = 0.2782nm$ and $\epsilon_{H_2-H_2}/k_b = 38.7K$. While classical results matched the experimental data at temperatures above 100K, below this temperature they predicted significantly higher diffusivities, confirming the importance of quantum effects below 100K. The zeolite structure was chosen to have a small window (0.543 nm) and the calculations again found the crossover selectivity, this time at around 94K. Below this temperature, D_2 starts diffusing faster than H_2 , the reason being the same steric hindrance as explained in their earlier work. The same reversal of kinetic selectivity was also experimentally supported by Zhao *et al* [16] where H_2 shows a slower adsorption kinetics compared to D_2 for temperatures around 77K, when carbon molecular sieves with pore dimension 0.546 nm and 0.566 nm were used. The authors finally conclude that the reverse kinetic selectivity is extremely sensitive to pore dimensions and advised a judicious choice of host material for practical applications.

In a recent article by Hankel *et al*[17], an effort was made to address the twin issue of advancing the modelling of quantum kinetic sieving by incorporating quantum

effects into classical simulations and searching for the actual occurrence of the "activation barrier" during molecular transport of hydrogen through macroporous materials. The methodologies used were the same as employed by Lu *et al*[9] which took care of the first issue as the molecules were treated as diatomics and therefore no quantum correction to the potential was needed. The basic model consisted of several connected pores with each pore mouth leading to a cavity and the kinetic sieving being influenced by both the pore mouth and the cavity. The pore mouths were made narrow enough to facilitate quantum kinetic sieving while the cavity was made large enough to accommodate the molecules and not hinder the transport between pore mouths. The H-C interaction was modelled by L-J potential with parameters $\epsilon = 19.2\text{cm}^{-1}$ and $\sigma = 3.08\text{\AA}$. As far as the activation barrier was concerned, the authors found that in the case of the tube shaped cavity models that they, the barrier in the cavity rather than in the pore mouth. Since the cavities would be of large diameter, the overall selectivity would be greatly reduced. If, however, spherical shaped cavities were considered the potential barrier could lie in the pore mouth provided the cavity was not too large. Though such a case would potentially make kinetic sieving possible, the flip side of such a structure is that the synthesis and control of both the shape and size of cavity as well as the size of the pore mouth is presently too challenging.

1.4 Our Aim

As is clear from a brief survey of the existing literatures on quantum molecular sieving, the effects have mostly been studied for a low temperature range and for a single nanotube. We sought to advance this idea and study the effect of molecular sieving by introducing a second nanotube. Thus instead of a single nanotube, we have a system of two nanotubes, with different radii, joined end to end. This model, according to us, should serve as a preliminary investigation into

how irregularities of the nanotube shape can affect molecular sieving. Along with the analytic treatment of this mathematical model, we also sought to inquire how a kinetic sieving of isotopes using carbon nanotubes compares with equilibrium sieving.

Chapter 2

THEORETICAL TOOLS

2.1 A brief discussion about carbon nanotube structures

The discussion in this section mainly follows the book by Reich, Thomsen and Maultzsch[18].

Carbon nanotubes are hollow cylinders of graphite sheets. A tube made of a single graphitic layer rolled up into a hollow cylinder is called a single-walled nanotube (SWNT), whereas a tube comprising several, concentrically arranged cylinders is referred to as a multiwall tube (MWNT). They can be looked at as single molecules, regarding their small size ($\sim nm$ in diameter and $\sim \mu$ in length), or as quasi-one dimensional crystals with translational periodicity along the tube axis. There are infinitely many ways to roll a sheet into a cylinder, resulting in different diameters and microscopic structures of the tubes. These are defined by the chiral angle i.e the angle of the hexagon helix around the tube axis.

In carbon nanotubes, the graphene sheet is rolled up in such a way that a graphene lattice vector $\vec{c} = n_1\vec{a}_1 + n_2\vec{a}_2$ becomes the circumference of the tube. This circumferential vector \vec{c} , which is usually denoted by the pair of integers (n_1, n_2)

, is called the chiral vector and uniquely defines a particular tube. For example, the (10, 10) tube contains 40 atoms in the unit cell and is metallic where as the close-by (10, 9) tube with 1084 atoms in the unit cell is a semiconducting tube.

The number of lattice points on the chiral vector is given by the greatest common divisor n of (n_1, n_2) , since $\vec{c} = n(n_1/n \cdot \vec{a}_1 + n_2/n \cdot \vec{a}_2)$ is a multiple of another graphene lattice vector \vec{c}' .

The direction of the chiral vector is measured by the chiral angle θ , which is defined as the angle between \vec{a}_1 and \vec{c} . The chiral angle θ can be calculated from

$$\cos\theta = \frac{\vec{a}_1 \cdot \vec{c}}{|\vec{a}_1| \cdot |\vec{c}|} = \frac{n_1 + n_2/2}{\sqrt{n_1^2 + n_1 n_2 + n_2^2}} \quad (2.1)$$

For each tube with θ between 0° and 30° an equivalent tube with θ between 30° and 60° is found, but the helix of graphene lattice points around the tube changes from right-handed to left-handed. Because of the six-fold rotational symmetry of graphene, to any other chiral vector an equivalent one exists with $\theta \leq 60^\circ$. We will hence restrict ourselves to the case $n_1 \geq n_2 \geq 0$ (or $0^\circ \leq \theta \leq 30^\circ$).

Tubes of the type $(n, 0)$ ($\theta = 0^\circ$) are called **zig-zag** tubes, because they exhibit a zig-zag pattern along the circumference. (n, n) tubes are called **armchair** tubes; their chiral angle is $\theta = 30^\circ$. Both, zig-zag and armchair tubes are achiral tubes, in contrast to the general chiral tubes.

The geometry of the graphene lattice and the chiral vector of the tube determine its structural parameters like diameter, unit cell, and its number of carbon atoms, as well as the size and the shape of the Brillouin zone. The diameter of the tube is given by the length of the chiral vector

$$d = \frac{|\vec{c}|}{\pi} = \frac{a_0}{\pi} \sqrt{n_1^2 + n_1 n_2 + n_2^2} = \frac{a_0}{N} \quad (2.2)$$

The smallest graphene lattice vector \vec{a} perpendicular to \vec{c} defines the translational period a along the tube axis. In general, the translational period a is determined

from the chiral indices (n_1, n_2) by

$$\vec{a} = \frac{2n_2 + n_1}{nR} \vec{a}_1 + \frac{2n_1 + n_2}{nR} \vec{a}_2 \quad (2.3)$$

and

$$a = |\vec{a}| = \frac{\sqrt{3(n_1^2 + n_1n_2 + n_2^2)}}{nR} a_0 \quad (2.4)$$

where $R = 3$ if $(n_1 - n_2)/3n$ is integer and $R = 1$ otherwise. Thus, the nanotube unit cell is formed by a cylindrical surface with height a and diameter d . For achiral tubes, eqn(2.2) and (2.4) can be simplified as

$$a_Z = \sqrt{3}a_0, |\vec{c}_Z| = na_0 \quad (\text{zigzag}) \quad (2.5)$$

$$a_A = a_0, |\vec{c}_A| = \sqrt{3}.na_0 \quad (\text{armchair}) \quad (2.6)$$

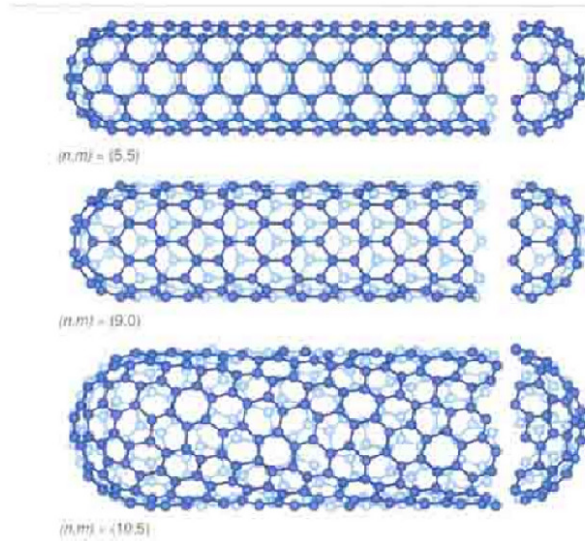


FIGURE 2.1: figure showing armchair, zigzag and chiral nanotubes respectively

The number of carbon atoms in the unit cell n , can be calculated from the area $S_t = a \cdot c$ of the cylinder surface and the area S_g of the hexagonal graphene unit cell. The ratio of these two gives the number q of graphene hexagons in the nanotube

unit cell

$$q = S_t/S_g = \frac{2\sqrt{n_1^2 + n_1n_2 + n_2^2}}{nR} \quad (2.7)$$

Since the graphene unit cell contains two carbon atoms, there are

$$n_C = 2q = \frac{4\sqrt{n_1^2 + n_1n_2 + n_2^2}}{nR} \quad (2.8)$$

carbon atoms in the unit cell of the nanotube. The results are summarised in table (2.1)

2.2 Energy eigenvalues for a particle in a square circular potential

The problem of a point mass in a one dimensional potential well is one of the most frequently solved problems in introductory quantum mechanics. On the one hand, the quantized energy levels can be easily understood in terms of simple wave mechanics argument involving fitting the de-broglie waves inside the box, while the position and momentum space wave functions can be intuitively correlated with behaviour of a particle bouncing back and forth in the well. The 2-D square well is one of the first examples of degeneracy due to symmetry ($L_x = L_y$) while the

TABLE 2.1: Structural parameters of armchair (*A*), zigzag (*Z*) and chiral (*C*) nanotubes

Type	Tube	N	$q = n_c/2$
<i>A</i>	(n, n)	$3n^2$	$2n$
<i>Z</i>	$(n, 0)$	n^2	$2n$
<i>C</i>	(n_1, n_2)	$\sqrt{n_1^2 + n_1n_2 + n_2^2}$	$2N/nR$
Type	diameter(d)	translational period(a)	chiral angle(θ)
<i>A</i>	$\sqrt{3}na_0/\pi$	a_0	30°
<i>Z</i>	na_0/π	$\sqrt{3}a_0$	0°
<i>C</i>	$\sqrt{N}a_0/\pi$	$\sqrt{3N}a_0/nR$	$\cos^{-1}[(n_1 + n_2/2)/\sqrt{N}]$

rectangular well, in certain cases, also give rise to accidental degeneracies. The 2-D circular infinite well can be used to introduce the quantum description of angular momentum and also exhibit degeneracies (due to the equivalence of clockwise and counter clockwise rotations). Since our proposed model will consist of a circular infinite well, in this section we briefly discuss the solutions for a general circular infinite well and its implications

2.2.1 Quantum Solutions

The quantum mechanical hamiltonian for a particle of mass μ inside a channel of radius \mathbf{R} is given by

$$H = \frac{-\hbar^2}{2\mu} \nabla^2 + V(\mathbf{r})$$

where

$$V(\mathbf{r}) = \begin{cases} 0 & \text{for } r < \mathbf{R} \\ +\infty & \text{for } r > \mathbf{R} \end{cases}$$

The time independent Schrödinger equation in such a case then merely reduces to Helmholtz equation, the radial part of which corresponds to the Bessel equation with the solution given by

$$E = \frac{\hbar^2}{2\mu R^2} [\lambda_{m,n}^2]$$

where $\lambda_{m,n}$ is the n^{th} zero of the m^{th} Bessel function, $n = n_r + 1$ and n_r counts the number of radial nodes in the wave function. Also,

$$L = (i/\hbar)(\partial/\partial\theta)$$

with eigenvalue $m\hbar$. Each state with non zero m is doubly degenerate due to the two equivalent values of $m = \pm|m|$ corresponding to clockwise and counter clockwise motion.

The behaviour of the wave functions can be discussed more concretely by examining the probability density for the radial co-ordinate, given by $P(r) = r|R(r)|^2$ with the normalization condition that

$$\int_0^R P(r)dr = 1$$

where the additional factor of r comes from the two dimensional measure for the polar co-ordinates. We can easily analyse the behaviour of two limiting cases-

1) For the generic case of $m=0$ and n_r large, we can make use of the asymptotic form (for $z=kr \gg 1$) of the regular bessel function, namely

$$J_n(z) \sim \sqrt{\frac{2}{\pi z}} \cos(z - n\pi/2 - \pi/4)$$

to note that

$$P_{(0, n_r \gg 1)}(r) \rightarrow r \left[\sqrt{\frac{2}{\pi kr}} \cos(kr - \pi/4) \right]^2 \propto \cos^2(kr - \pi/4)$$

This is quite similar to the case of a one dimensional well where the particle would bounce back and forth across a diameter through the origin.

2) For the case of purely angular motion, $m \gg 1$ and $n_r=0$, we can make use of a general variational wave function to examine the limiting behaviour. We can use

$$R_m(r; \alpha) = r^{|m|} (R^\alpha - r^\alpha)$$

where α is the variational parameter. This form incorporates the appropriate boundary conditions at $r=0$ [where $R(r) \rightarrow r^m$ due to the angular momentum barrier] and at $r=R$ and has no radial nodes; it will provide a lower boundary to the energy of the $n_r=0$ state for each value of m . The energy functional given

by this trial wave function is

$$E_m(\alpha) = E(R_m(r, \alpha)) = \frac{\hbar^2}{2\mu R^2} [(m+1) \frac{(2m+\alpha+2)(m+\alpha+1)}{m+\alpha}]$$

which has a minimum for $\alpha = \sqrt{m+2} - m$ for each value of m . Using this functional form as a guide, we can easily find that in the large m limit, we have for the average of r

$$\langle r \rangle \rightarrow R(1 - 1/2\sqrt{m} - 3/4m + \dots)$$

and

$$\langle r \rangle^2 = R^2(1 - 1/\sqrt{m} - 1/m + \dots)$$

so that

$$\Delta r = \sqrt{\langle r \rangle^2 - \langle r^2 \rangle} \rightarrow \frac{R}{2\sqrt{m}}$$

and the limit for purely rotational motion, strongly peaked near the radius in the rim, is evident for $m \gg 1$.

2.2.2 Classical probability distribution for position

The classical probability distribution for position $P_{Cl}(x)$ can be defined by averaging over many measurements of the co-ordinates along a classical trajectory. A similar quantity for the radial co-ordinate can be derived for comparison with $P_{Qm}(r) = r^{-2}$ by considering a classical expression for E , in terms of the radial co-ordinate and the conserved angular momentum L . According to Robinett[19]

$$E = \frac{1}{2}\mu(dr/dt)^2 + \frac{L^2}{2\mu r^2}$$

This gives,

$$\frac{dr}{dt} = \sqrt{\frac{2}{\mu} \left(E - \frac{L^2}{2\mu r^2} \right)} \Rightarrow dt = \sqrt{\frac{\mu}{2E}} \frac{r dr}{\sqrt{r^2 - R_{min}^2}}$$

where $R_{min} = \sqrt{\frac{L^2}{2\mu E}}$ is the distance of closest approach to the origin.

Using the standard argument that the probability of finding the particle in the radial interval $(r, r+dr)$ is proportional to the small time dt spent in the region, one makes the association $P_{Cl}(r)dr = dt / (\tau/2)$ where τ is the period of motion.

For the radial variable we then find that

$$\tau_r = \sqrt{\frac{2\mu}{E}} \sqrt{R^2 - R_{min}^2}$$

and

$$P_{Cl}(r) = \frac{r}{\sqrt{R^2 - R_{min}^2} \sqrt{r^2 - R_{min}^2}}$$

The limit of purely radial motion corresponds to $R_{min}=0$ so that $\tau = \sqrt{\frac{2\mu R^2}{E}} = 2R/v$ as expected while $P_{Cl}(r) = 1/R$ corresponding to uniform probability of finding the particle at any point on a given radius, again, similar to the one dimensional box.

2.3 Bessel functions: Introduction, few properties and recurrence relation

In our calculations we have extensively used Bessel functions and their properties. This section is hence devoted to the discussion of Bessel functions and few of their important properties [20].

2.3.1 Bessel functions of the first and second kind

Bessels equation is an ordinary, linear, homogeneous differential equation given by

$$x^2 y'' + xy' + (x^2 - m^2)y = 0 \quad (2.9)$$

and gives rise to a solution that is a linear combination of a Bessel function of order m (m is positive) denoted by $J_m(x)$ and a Neumann function of order m denoted by $Y_m(x)$.

We note that the solutions of eq(2.9) is of the form

$$f(x) = \sum_{n=0}^{\infty} a_n x^{n+s} \quad (2.10)$$

and we proceed to obtain the solution via Frobenius' method.

To determine s for a second order homogenous differential equation, one must set eq(2.10) equal to the dependent variable and take appropriate derivatives and then equate all coefficients to zero. After doing so, one will get a quadratic relationship for s (giving two roots s_1 and s_2) known as the indicial equation. Now two situations may arise-

- 1) If s_1 and s_2 are distinct and do not differ by an integer, then there are two linearly independent solutions of both of the form of (2.10)
- 2) If s_1 and s_2 are distinct but do differ by an integer, one must use an important fact from differential equations which states that if one solution is found, y_1 , then a second may be found by

$$y_2(x) = y_1(x) \int \frac{\exp(-\int P(x)dx)}{y_1^2(x)} dx \quad (2.11)$$

This equation can be manipulated thus finally giving

$$y_2(x) = Cy_1(x) \ln(x) + \sum_{n=0}^{\infty} b_n x^{n+s_2} \quad (2.12)$$

3) If s_1 and s_2 are degenerate roots of the indicial equation, then one must find a second solution of the form of (2.12).

Making the substitution of (2.12), as well as appropriate derivatives into (2.10), we can get the indicial equation that has concerned us to be $(s_2 - m_2)a_0 = 0$ which implies that $s = \pm m$. This means that case (1) applies to us when $2m \neq$ integer or $m \neq$ one half of an integer, case (3) applies when $m = 0$ and case (2) applies for any other m .

Lets initially consider the case of $+m$ to get our first solution (which will turn out to be the Bessel functions). After completing the Frobenius method, one of the solutions is found to be

$$J_m(x) = \sum_{n=0}^{\infty} \frac{(-1)^n}{n! \Gamma(m+n+1)} \left(\frac{x}{2}\right)^{2n+m} \quad (2.13)$$

where $\Gamma(m+n+1)$ is known as the gamma function and is defined by $\Gamma(n+1) = n!$ To get a second linearly independent function we must first consider the nature of m . As discussed previously, if m is not either an integer or a half integer, we know that it fits into the case 1 category. This means that our general solution (which must include a linear combination of two linearly independent functions) is of the form

$$y_1 = C_1 J_m(x) + C_2 J_{-m}(x) \quad (2.14)$$

From here, we have two special circumstances where a case 2 scenario may arise. The first circumstance is where m is a half and odd integer. In this case the solutions reduce to linear combinations of sine and cosine functions. This is an example of a case where the difference in the s values is an integer, but we still get two linearly independent functions of the form of (2.12). The case where m is a half integer is called spherical bessel function. In our dicussion, we will limit ourselves to the situations where m is integer and not bother ourselves with spherical bessel functions.

We are looking for the relationship between J_m and J_{-m} where $m = 1, 2, 3, \dots$ (we have considered m as non negative). Putting this into the series representation of the Bessel function, we see that

$$J_{-m}(x) = \sum_{n=0}^{\infty} \frac{(-1)^n}{n! \Gamma(-m + n + 1)} \left(\frac{x}{2}\right)^{2n-m} \quad (2.15)$$

However since Gamma function is not defined for negative integers, we can further modify the above result as

$$J_{-m}(x) = \sum_{n=m}^{\infty} \frac{(-1)^n}{n! \Gamma(-m + n + 1)} \left(\frac{x}{2}\right)^{2n-m}$$

.

If we wish to start the series from $n = 0$, a new variable $z = n - m$ can be defined and after some manipulation one finally obtains

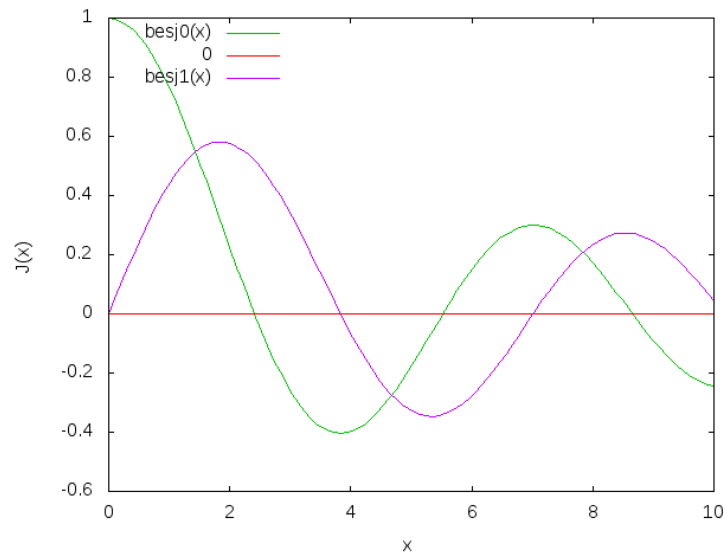
$$J_{-m}(x) = (-1)^m J_m(x) \quad (2.16)$$

which gives the relation between $J_m(x)$ and $J_{-m}(x)$.

The other solution $Y_m(x)$ is generally given by

$$Y_m(x) = \lim_{p \rightarrow m} \frac{\cos(p\pi) J_p - J_{-p}}{\sin p\pi} \quad (2.17)$$

Now that two linearly independent solutions have been presented that will cover any order Bessel function, we can explore some of the properties of these mathematical functions. From the form of (2.16), we can conclude that a Bessel function of an odd integer order is considered an odd function while a Bessel function of an even integer order is an even function. Also, it is useful to derive the following relationship between Bessel functions of different orders and their respective derivatives.

FIGURE 2.2: $J_m(x)$ for first few orders (note the continuity at origin)

$$\frac{d}{dx} \left(\frac{J_m(x)}{x^m} \right) = \frac{-J_{m+1}}{x^m} \quad (2.18)$$

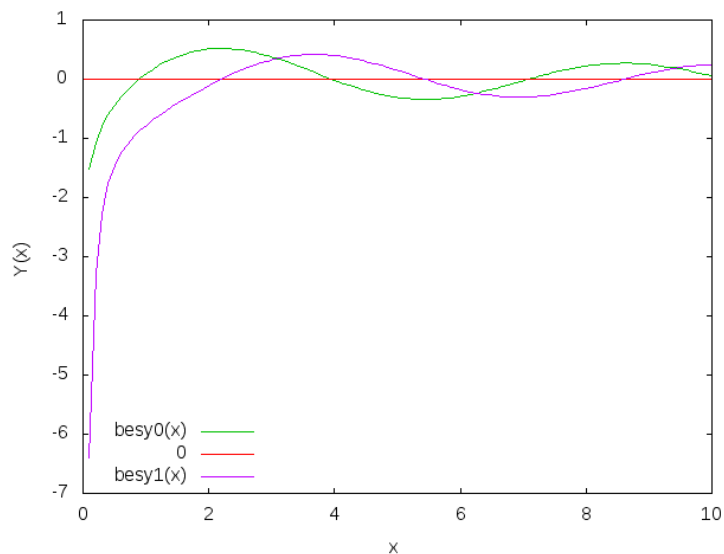
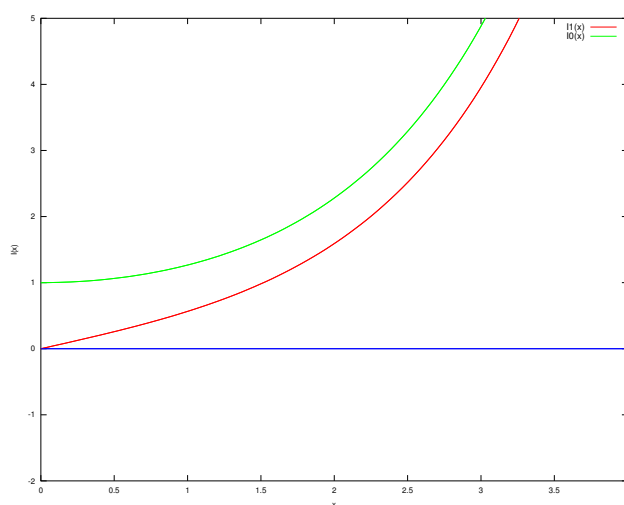
$$\frac{d}{dx} (x^m J_m(x)) = x^m J_{m-1}(x) \quad (2.19)$$

One special case of (2.19) is when it applies to $J_0(x)$. Here, since $m=0$, we have,

$$\frac{d}{dx} J_0(x) = -J_1(x) \quad (2.20)$$

From the diagram of $J_m(x)$ we can see that like trigonometric functions, $J_m(x)$ have infinitely many zeros and it can be shown that spacing between these zeros approach π (however, the zeros of the function are not spaced by the same amounts as they are in trigonometric functions). Also, like the cosine function, $J_0(0) = 1$ while like the sine function $J_1(0) = 0$

Also from the diagram for $Y_m(x)$, we notice how the function is unbounded at origin, contrary to $J_m(x)$. Hence, for well behaved solutions at origin, we must only consider $J_m(x)$. (as we have done throughout our calculations to follow)

FIGURE 2.3: $Y_m(x)$ for first few orders (note the singularity at origin)FIGURE 2.4: $I_m(x)$ for first few orders (note continuity at origin)

2.3.2 Modified Bessel functions

If the form of eqn.(2.9) is changed by the transformation $x \rightarrow ix$, it reduces to

$$x^2 y'' + xy' - (x^2 + m^2)y = 0 \quad (2.21)$$

the solutions of eq(2.21) are Bessel functions of imaginary argument. The solution which is regular at the origin(analogous to $J_m(x)$) is

$$I_m(x) = i^{-m} J_m(ix) \quad (2.22)$$

It is also often represented as

$$I_m(x) = e^{-m\pi i/2} J_m(xe^{i\pi/2}) \quad (2.23)$$

The series representation of $I_{\pm m}(x)$ is given as

$$I_{\pm m}(x) = \sum_0^{\infty} \frac{1}{s!(s \pm m)!} \left(\frac{x}{2}\right)^{2s \pm m} \quad (2.24)$$

For integral m ,

$$I_m(x) = I_{-m}(x) \quad (2.25)$$

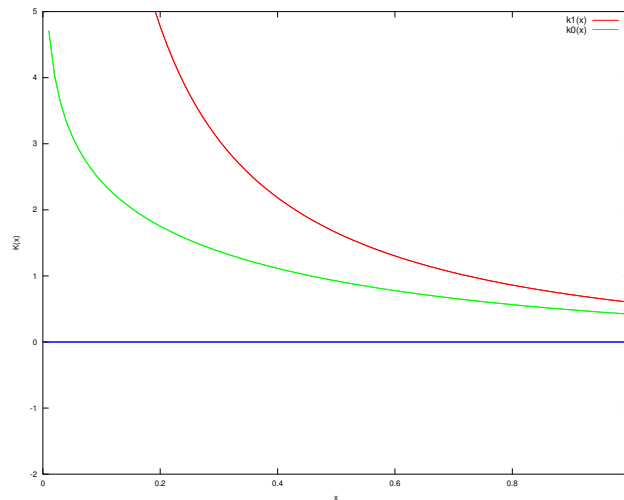
A second solution to eqn.(2.21)is also considered on basis of its asymptotic behaviour and is given as

$$K_m(x) = \frac{\pi}{2} \frac{I_m(x) - I_{-m}(x)}{\sin m\pi} \quad (2.26)$$

2.3.3 Recurrence relations

This section lists a few useful recurrence relations between the Bessel functions that have been used in future calculations, especially the relation among the derivatives.

$$\frac{d}{dx}(x^m J_m(x)) = x^m J_{m-1}(x) \quad (2.27)$$

FIGURE 2.5: $K_m(x)$ for first few orders (note the singularity at origin)

$$\frac{d}{dx} J_0(x) = -J_1(x) \quad (2.28)$$

$$\frac{d}{dx} (x^m Y_m(x)) = x^m Y_{m-1}(x) \quad (2.29)$$

$$\frac{d}{dx} Y_0(x) = -Y_1(x) \quad (2.30)$$

$$J'_m(x) = \frac{1}{2} [J_{m-1}(x) - J_{m+1}(x)] \quad (2.31)$$

$$Y'_m(x) = \frac{1}{2} [Y_{m-1}(x) - Y_{m+1}(x)] \quad (2.32)$$

$$\frac{d}{dx} I_0(x) = I_1(x) \quad (2.33)$$

$$\frac{d}{dx} K_0(x) = -K_1(x) \quad (2.34)$$

$$I'_m(x) = \frac{1}{2} [I_{m-1}(x) + I_{m+1}(x)] \quad (2.35)$$

$$-K'_m(x) = \frac{1}{2} [K_{m-1}(x) + K_{m+1}(x)] \quad (2.36)$$

2.4 Maxwell-Boltzmann Distribution

The Maxwell-Boltzmann distribution is the classical probability distribution function for distribution of molecular speed, momenta or energy between identical but distinguishable particles and applies to ideal gases close to thermodynamic equilibrium with negligible quantum effects and at non-relativistic speeds. The derivation of the distribution can be readily seen from the Maxwell-Boltzmann statistics where the expected number of particles with energy ϵ_i is given as

$$N_i = \frac{g_i}{e^{(\epsilon_i - \mu)/k_b T}} = \frac{N}{Z} g_i e^{-\epsilon_i/k_b T} \quad (2.37)$$

where

- N_i is the number of particles in state i
- ϵ_i is the energy of the i^{th} state
- g_i is the degeneracy of energy level i
- μ is the chemical potential
- k_b is Boltzmann's constant
- T is absolute temperature
- $N = \sum N_i$ is the total number of particles
- $Z = \sum g_i e^{-\epsilon_i/k_b T}$ is the *partition function*

2.4.1 Distribution for the momentum vector

For the case of an "ideal gas" consisting of non-interacting atoms in the ground state, all energy is in the form of kinetic energy, and g_i is constant for all i . The

relationship between kinetic energy and momentum for massive particles is

$$\epsilon = \frac{p^2}{2m} \quad (2.38)$$

where p^2 is the square of the momentum vector $\vec{p} = [p_x, p_y, p_z]$. Eqn(2.37) thus becomes

$$\frac{N_i}{N} = \frac{1}{Z} \exp \left[-\frac{p_{i,x}^2 + p_{i,y}^2 + p_{i,z}^2}{2mk_bT} \right] \quad (2.39)$$

This distribution of N_i/N is proportional to the probability density function f_p for finding a molecule with these values of momentum components, so

$$f_p(p_x, p_y, p_z) = \frac{c}{Z} \exp \left[-\frac{p_x^2 + p_y^2 + p_z^2}{2mk_bT} \right] \quad (2.40)$$

and the normalizing constant c is given as $c = \frac{Z}{(2\pi mk_bT)^{3/2}}$ and the final distribution looks like

$$f_p(p_x, p_y, p_z) = \frac{1}{(2\pi mk_bT)^{3/2}} \exp \left[-\frac{p_x^2 + p_y^2 + p_z^2}{2mk_bT} \right] \quad (2.41)$$

The distribution is seen to be the product of three independent normally distributed variables p_x, p_y, p_z , with variance mk_bT . Additionally, it can be seen that the magnitude of momentum will be distributed as a MaxwellBoltzmann distribution, with $a = \sqrt{mk_bT}$.

2.4.2 Distribution for velocity

The velocity probability density f_v is proportional to the momentum probability density function by

$$f_v d^3v = f_p \left(\frac{dp}{dv} \right)^3 d^3v \quad (2.42)$$

Using $\vec{p} = m\vec{v}$ we get

$$f_v(v_x, v_y, v_z) = \frac{m}{(2\pi k_bT)^{3/2}} \exp \left[-\frac{m(v_x^2 + v_y^2 + v_z^2)}{2mk_bT} \right] \quad (2.43)$$

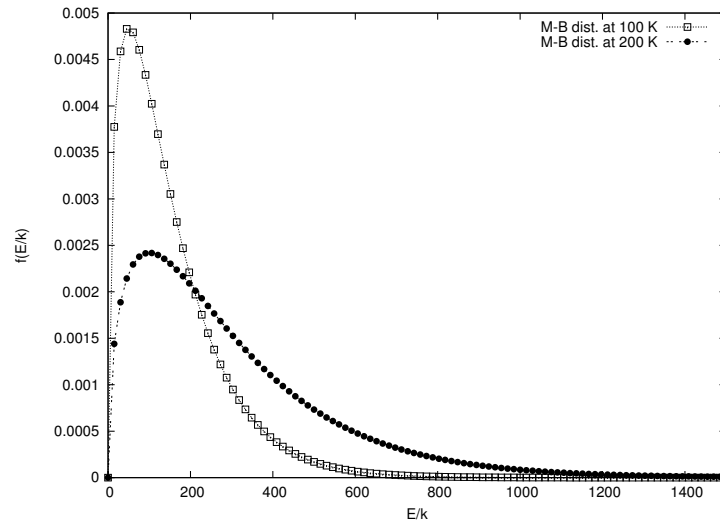


FIGURE 2.6: Maxwell-Boltzmann energy distribution for two different temperatures

The probability of finding a particle with velocity in the infinitesimal element $[dv_x, dv_y, dv_z]$ about velocity $v = [v_x, v_y, v_z]$ is $f_v(v_x, v_y, v_z) dv_x dv_y dv_z$. Like the momentum, this distribution is also the product of three independent normally distributed variables v_x, v_y, v_z , but with variance $\frac{k_b T}{m}$.

Chapter 3

THEORETICAL MODEL

Our theoretical model, as mentioned before, consists simply of a two nanotube system with unequal radii that are joined end to end. Let us denote the radii of the two channels as a and b ($a > b$). The nanotube with the wider radius is at the bottom while the narrower one is at the top. The system as whole is connected to two reservoirs, one at both ends. The reservoir at the bottom (the one connected to the wider nanotube) has a mixture of H_2 and D_2 isotopes in equilibrium. Next we allow the molecules to enter the nanotube system and we make the following crucial assumption. *The molecules that are inside the nanochannel have a free classical motion along the axis of the tube, but are confined in a potential well along the radial plane. The potential well arises due to the interaction of the molecules with walls of the nanochannel.* We are interested in finding out the final percentage of each isotope that is allowed to go through the system and end up in the second reservoir on the top. In the following sections, a systematic approach to developing such a model is given.

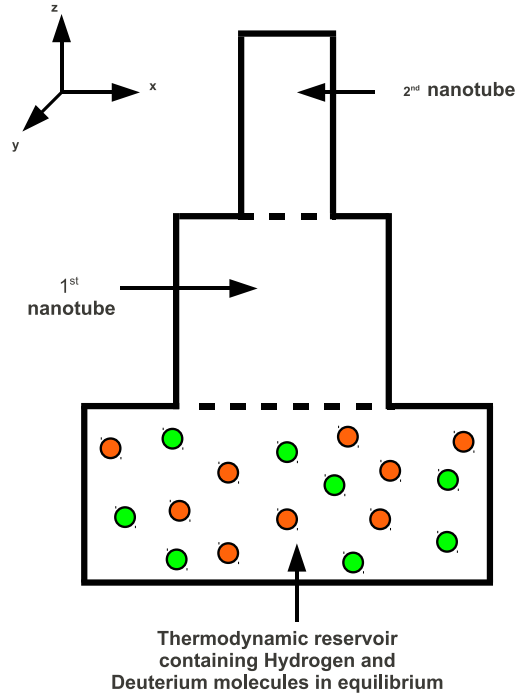


FIGURE 3.1: a rough sketch of the theoretical model

3.1 From reservoir to nanochannel

We considered previously that outside the channel the gas molecules are in a kind of thermodynamic reservoir in equilibrium having all possible energies. Therefore it is natural to assume that they are distributed according to the Maxwell-Boltzmann distribution.

The Maxwell-boltzmann distribution for velocity is given by

$$f^3(v)d^3v = \left(\frac{\mu}{2\pi k_b T}\right)^{\frac{3}{2}} \exp(-\mu v^2/2k_b T)d^3v \quad (3.1)$$

where $v^2 = v_x^2 + v_y^2 + v_z^2$

$d^3v = dv_x dv_y dv_z$ is the volume element in cartesian co-ordinates. It is noted that the axial direction coincides with the z axis while the radial plane lies along $x - y$ direction.

We can consider the above equation as being a product of 3 independent one dimensional equations. Now, instead of cartesian coordinates, we turn our attention to cylindrical coordinates.

Then, $v^2 = v_\rho^2 + v_\theta^2 + v_z^2$ and the relation between cylindrical and cartesian coordinate is given by $x = \rho \cos(\theta), y = \rho \sin(\theta), z = z$. The volume element in this case becomes $d^3v = \rho dv_\rho dv_\theta dv_z$ where the prefactor ρ is the jacobian of the coordinate transformation.

As before, we can consider the distribution as a product of three separate distributions with the distribution along \vec{z} in particular given as

$$f(v_z)dv_z = \left(\frac{\mu}{2\pi k_b T} \right)^{\frac{1}{2}} \exp(-\mu v_z^2 / 2k_b T) dv_z \quad (3.2)$$

which is the same as in cartesian case, as the transformation of the z axis is same in both cases.

As per our assumption, the molecule propagates along the \vec{z} direction, i.e the axis of the nanotube, unhindered (like a classical gas). Hence we expect its energy to be the same as that outside the channel, unaffected by the quantum restrictions which apply only along the radial direction i.e $\rho - \theta$ plane.

So the component of the distribution along \vec{z} should be the same in both classical case (outside tube) and the confinement case (inside tube). More specifically, we want the distribution for the energy in preference to the distribution for velocity. We want to quantize the distribution along v_x and v_y while keeping v_z fixed i.e we want to evaluate the integral $f(v_x)f(v_y)dxdy$. We transform to the polar coordinates to evaluate the integral easily.

$$x = \rho \cos(\theta), y = \rho \sin(\theta) \text{ and } v_x = v_\rho \cos(\theta), v_y = v_\rho \sin(\theta).$$

Therefore the distribution now becomes-

$$\begin{aligned} f(v_x)f(v_y)dxdy &= \left(\frac{\mu}{2\pi k_b T}\right) \exp(-\mu(v_x^2 + v_y^2)/2k_b T)dxdy \\ &= \left(\frac{\mu}{2\pi k_b T}\right) \exp(-\mu v_\rho^2/2k_b T)v_\rho dv_\rho d\theta \end{aligned}$$

Because of isotropy, the equation can be integrated over θ leaving us with distribution along x-y plane as

$$f(v_\rho)dv_\rho = \frac{\mu}{k_b T} \exp(-\mu v_\rho^2/2k_b T)v_\rho dv_\rho$$

with($v_\rho \geq 0$)

However, since we are more interested in the energy distribution, we transform the distribution by setting $E_\rho = (1/2)\mu v_\rho^2$ and $dE_\rho = \mu v_\rho dv_\rho$.

So the distribution in terms of energy becomes

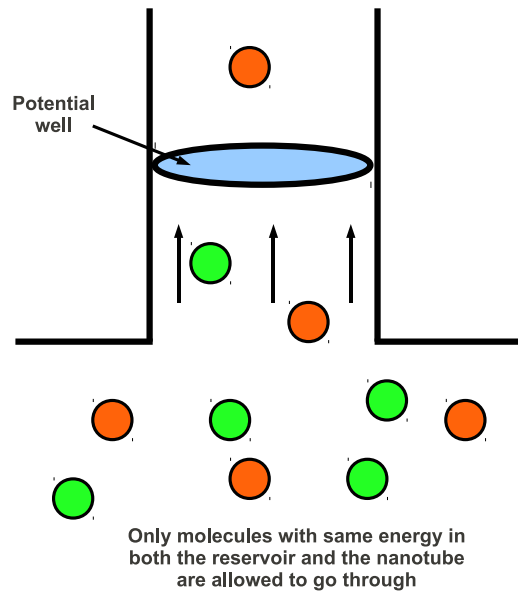


FIGURE 3.2: a sketch of how the molecules proceed from the reservoir to the first nanochannel

$$f(E_\rho)dE_\rho = \frac{1}{k_b T} \exp(-E_\rho/k_b T) dE_\rho \quad (3.3)$$

Simplifying the equation further by defining $E_\rho/k_b = E'_\rho$, we get

$$f(E'_\rho)dE'_\rho = \frac{1}{T} \exp(-E'_\rho/T) dE'_\rho \quad (3.4)$$

Now, inside the channel we have

$$\begin{aligned} k_x + k_y + V &= E_n \\ \Rightarrow \frac{(v_x^2 + v_y^2)}{2\mu} + V &= E_n \\ \Rightarrow \mu v_\rho^2/2 + V &= E_n \\ \Rightarrow E_\rho + V &= E_n \\ \Rightarrow E_\rho = E_n - V &= \tilde{E} \\ \Rightarrow E'_\rho = E_n/k_b - V/k_b &= \tilde{E}/k_b = \tilde{E}' \end{aligned}$$

Therefore, to calculate the percentage of particles that are allowed into the channels, we have to integrate the distribution $f(E'_\rho)dE'_\rho$ between the limits $\tilde{E}' - \Delta\tilde{E}'$ and $\tilde{E}' + \Delta\tilde{E}'$. The limits arise because the nanotube radius may not be exactly smooth (with a variation of Δr), and hence a variation of radius will eventually lead to a slightly varying energy level. To smooth out these effects and for a more accurate approximation, it is imperative to integrate within a limit, rather than calculating the percentage corresponding to a fixed energy value.

3.2 Quantized energy levels in the nanochannels

In this section, we consider the quantization of energy levels of the confined molecules inside the nanochannels. As mentioned earlier, the molecules are confined inside an infinite potential well of depth ϵ that is created due to the interaction between the molecules and the nanotube walls. The channel radius is denoted by \mathbf{R} .

The Hamiltonian for a particle of mass μ in such a case is given by

$$H = -\frac{\hbar^2}{2\mu}\nabla^2 + V(\mathbf{r})$$

where

$$V(\mathbf{r}) = \begin{cases} -\epsilon & \text{for } r < \mathbf{R} \\ +\infty & \text{for } r > \mathbf{R} \end{cases}$$

The corresponding stationary Schrödinger equation thus reduces to

$$(\nabla^2 + k^2)\psi(r, \theta) = 0 \tag{3.5}$$

where

$$k^2 = \frac{2\mu(\mathbf{E} + \epsilon)}{\hbar^2}$$

with the boundary condition that

$$\psi(R, \theta) = 0$$

(since the molecules are confined inside the tube, hence the wavefunctions must vanish at the boundary). Here we have two channels of radius a and b and we solve the Schrödinger equation independently for both channels. Because of the

circular symmetry, the solution can be written in the separable form

$$\psi(r, \theta) = R(r)\Theta_m(\theta)$$

where

$$\Theta_m(\theta) = \frac{1}{\sqrt{2\pi}}e^{im\theta}$$

for $m = 0, \pm 1, \pm 2, \dots$. The resulting radial equation is

$$\frac{d^2 R}{dr^2} + \frac{1}{r} \frac{dR}{dr} + \left(k^2 - \frac{m^2}{r^2}\right)R = 0 \quad (3.6)$$

which can be recognized as the Bessel's equation in variable $z = kr$. We want only those solutions which are well-behaved at the origin which are $J_{|m|}(kr)$ with the energy eigenvalues being determined by the boundary condition i.e $R(r)\Theta_m(\theta) = 0 \Rightarrow J_{|m|}(kr) = 0$. The solution to this equation is given by

$$E_{m,n} = -\epsilon + \frac{\hbar^2}{2\mu R^2}[\lambda_{m,n}^2] \quad (3.7)$$

where $\lambda_{m,n}$ is the n^{th} zero of the m^{th} Bessel function. Each state with non zero m is doubly degenerate due to the two equivalent values of $\pm|m|$, for every integer m .

As mentioned earlier, we have a two nanotube system with radii a and b respectively. We solve the quantized energies for both channels independently and then claim the following. *A molecule is allowed to travel to the second channel through the first channel only when its quantized energies overlap (within a given tolerance) in both channels.*

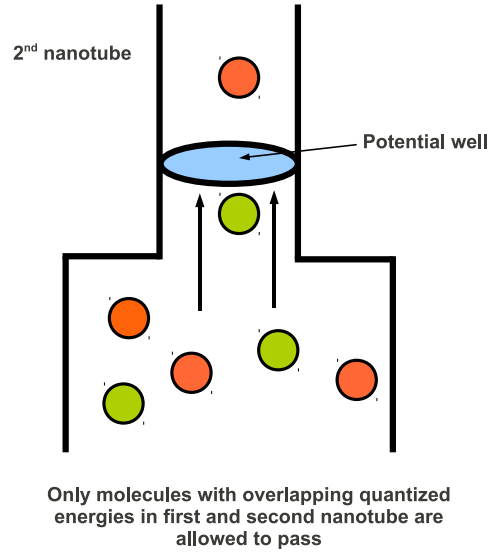


FIGURE 3.3: a sketch of how the molecules proceed through the nanotubes

To be more precise, we provide a theoretical treatment of the facts provided above. For two radii a and b , if we want overlapping energy levels, we have

$$E_{k,l}^1 = E_{m,n}^2 \implies \left(\frac{\lambda_{k,l}}{a} \right)^2 = \left(\frac{\lambda_{m,n}}{b} \right)^2$$

As such an exact equality is too hard to satisfy. But considering the fact that the channel radii and the molecular energies are only approximately fixed, we allow a tolerance δ of the energy levels and look for a correspondence within that tolerance:

$$E_{m,n}^2 - \delta \leq E_{k,l}^1 \leq E_{m,n}^2 + 2\delta \quad (3.8)$$

In terms of Bessel zeroes, this becomes

$$\left| \left(\frac{\lambda_{k,l}}{a} \right)^2 - \left(\frac{\lambda_{\mu,n}}{b} \right)^2 \right| \leq \frac{4\mu\delta^2}{\hbar}$$

where μ is the mass.

Also, we must take $k = m$ as the angular momenta of the molecules don't change while they travel from one channel to the other. In other words, we look for correspondences of energy between molecules of same angular momentum. The smoothness of the dependence of bessel zeroes on parameters implies the existence of a $\chi_{m,n} > 0$ such that the condition is verified for

$$\left| \left(\frac{\lambda_{m,n}}{a} \right)^2 - \left(\frac{\lambda_{m,n}}{a + \chi} \right)^2 \right|$$

for a fixed m, n if $\chi_{m,n} < \chi$.

Chapter 4

RESULTS

In this section. we discuss in details the results obtained from our calculations and their implications.

4.1 Calculation of energy levels

Following the discussions of section 3.2, we try to calculate the energy levels inside of a nanotube whose width is fixed at $1nm$. The molecules are constrained to move inside a potential well with $\epsilon/k_b = -200K$. The remaining parameters for are given as μ_H (mass of hydrogen)= $3.348 \times 10^{-27} Kg$, μ_D (mass of deuterium)= $12.025 \times 10^{-27} Kg$ and $\hbar = 1.0546 \times 10^{-34} Js$. We consider the solution of the Helmholtz equation given in the preveious chapter for $m = 0, 1, 2...5$ and list the first few energy levels for hydrogen and deuterium following eq(3.6). It is pertinent to note that the energy levels are independent of temperature

From the tables 4.1 and 4.2, it is clear that the energy levels of deuterium are far more closely spaced than that of hydrogen. Actually, from eq (3.6) it is evident that

TABLE 4.1: energy levels (in K) for hydrogen for various m values

E_n	$m = 0$	$m = 1$	$m = 2$	$m = 3$	$m = 4$	$m = 5$
E_0	-199.304	-198.233	-196.827	-195.103	-193.072	-190.744
E_1	-196.334	-194.079	-191.476	-188.537	-185.271	181.684
E_2	-190.990	-187.548	-183.756	-179.620	-175.148	-170.345
E_3	-183.272	-178.643	-173.662	-168.335	-162.666	-156.660
E_4	-173.180	-167.363	-161.194	-154.677	-147.815	-140.612
E_5	-160.712	-153.708	-146.352	-138.646	-130.593	-122.197
E_6	-145.870	-137.678	-129.134	-120.240	-110.100	-101.400
E_7	-128.652	-119.274	109.542	99.460	-89.029	-78.251
E_8	109.061	-98.494	87.576	76.305	64.685	-52.718
E_9	-87.094	-75.340	-63.234	-50.776	-37.968	-24.811

increasing the mass of the molecule increases the proximity of corresponding energy levels ,in agreement with the correspondence principle of quantum mechanics.

4.2 Inside the first nanochannel

In section 3.1 ,we have already derived an expression for the number density of the molecules inside the first nanotube travelling from the thermal reservoir. Here we try to give a numerical estimate of the percentage of particles that can be inside the first nanotube following eqn (3.4). $\Delta\tilde{E}'$ is taken to be 1 K for our calculations ($\Delta\tilde{E}' \approx \Delta r$ from eqn (3.7)). In table 4.3, an estimate of the percentage of Hydrogen molecules(in units of 10^{-3}) that are allowed to pass into the first nanochannel of width 1 nm(at room temperature T=300 K) for various m values are displayed.

TABLE 4.2: energy levels (in K) for deuterium for various m values

E_n	m=0	m=1	m=2	m=3	m=4	m=5
E_0	-199.652	-199.116	-198.411	-197.548	-196.531	-195.366
E_1	-198.165	-197.035	-195.732	-194.261	-192.626	-190.830
E_2	-195.489	-193.767	-191.867	-189.796	-187.557	-185.152
E_3	-191.625	-189.307	-186.813	-184.146	-181.308	-178.301
E_4	-186.572	-183.659	-180.571	-177.308	-173.872	-170.266
E_5	-180.330	-176.823	-173.140	-169.281	-165.250	-161.046
E_6	-172.898	-168.797	-164.519	-160.066	-155.439	-150.639
E_7	-164.278	-159.582	-154.710	-149.662	-144.440	-139.043
E_8	-154.469	-149.179	-143.712	-138.069	-132.252	-126.260
E_9	-143.471	-137.586	-131.525	-125.287	-118.875	-112.288

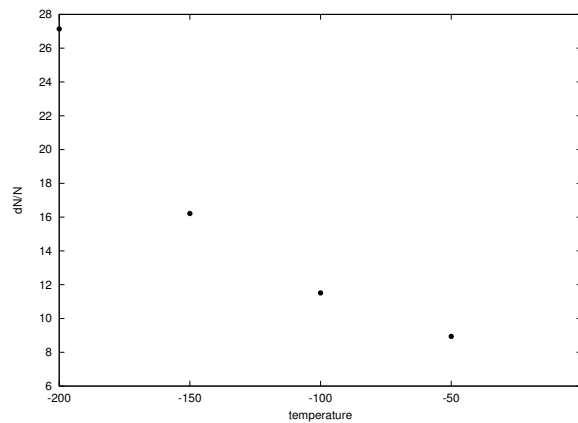
TABLE 4.3: percentage of hydrogen(in units of 10^{-3}) inside first nanotube for various m values

E_n	m=0	m=1	m=2	m=3	m=4	m=5
E_0	6.651	6.627	6.596	6.559	6.514	6.464
E_1	6.586	6.556	6.480	6.417	6.347	6.272
E_2	6.469	6.396	6.315	6.229	6.344	6.039
E_3	6.305	6.208	6.106	5.999	5.886	5.770
E_4	6.096	5.979	5.858	5.732	5.603	5.469
E_5	5.848	5.713	5.575	5.434	5.289	5.144
E_6	5.566	5.416	5.264	5.110	4.940	4.799
E_7	5.256	5.094	4.931	4.768	4.605	4.443
E_8	4.923	4.753	4.583	4.414	4.246	4.080
E_9	4.576	4.400	4.226	4.054	3.885	3.718

TABLE 4.4: percentage of hydrogen(in units of 10^{-3}) inside first nanotube for various temperature (m is fixed at 0)

E_n	T=-200	T=-100	T=-50	T=0
E_0	27.138	11.514	8.941	7.307
E_1	26.056	11.318	8.822	7.228
E_2	24.217	10.974	8.613	7.088
E_3	21.787	10.495	8.320	6.891
E_4	18.974	9.900	7.952	6.641
E_5	15.995	9.212	7.520	6.344
E_6	13.052	8.455	7.034	6.008
E_7	10.310	7.654	6.513	5.641
E_8	7.883	6.834	5.965	5.251

In the next two tables 4.4 and 4.5, a comparative study of the percentage of hydrogen and deuterium molecules (for a fixed m value, in this case taken to be zero) that are allowed inside the channel with respect to varying temperature (in Celsius) are given.

FIGURE 4.1: dN/N vs temperature(in Celsius)for ground state energy($m = 0$)

From the table 4.3, we see that lower energy levels allow for more molecules at low temperatures and this trend gets reversed as the temperature is increased. This makes sense physically as we expect the low energy states to dominate at lower temperatures whereas with increase of temperature more and more higher energy levels come to play. As a result, the percentage of molecules entering into the channel with high energies increase as the temperature is increased

TABLE 4.5: percentage of deuterium(in units of 10^{-3}) inside first nanotube for various temperature (m is fixed at 0)

E_n	T=-200	T=-150	T=-100	T=0
E_0	27.267	16.214	11.537	7.317
E_1	26.718	16.019	11.439	7.277
E_2	25.756	15.675	11.263	7.206
E_3	24.283	15.190	11.014	7.015
E_4	22.795	14.579	10.697	6.974
E_5	20.926	13.857	10.318	6.817
E_6	18.901	13.045	9.884	6.634
E_7	16.796	12.162	9.404	6.427
E_8	14.684	11.230	8.886	6.201
E_9	12.630	10.269	8.338	5.956

4.3 Inside the second channel

Now, we concentrate on the second channel and try to calculate the energy levels inside it for both hydrogen and deuterium by varying the width of the channel from 0.9 nm to 0.1 nm following equation (3.4). For two tubes of width of 1nm each it is evidently equivalent of having a single nanotube. Two tables showing the first few energy levels for both hydrogen and deuterium with $m = 0$ are given in tables 4.6 and 4.7.

If we compare the energy levels in the narrower channel for both hydrogen and deuterium, we find that the probability of coincidence of energy levels between the two channels in deuterium is much higher than that in case of hydrogen. This

means that deuterium is more likely to pass into the second channel as compared to that of hydrogen, especially at lower temperatures. Here in lies the uniqueness of the sieving device. If it was a single nano channel, isotopic sieving would have been due to the difference in zero point energy (which occurs because of the difference in mass). However, with the addition of a second nanochannel, narrower in width than the first one, the prediction of this model is that there appears to be another possibility of sieving which is based on energy. By tuning the right energy levels, we can determine the percentage of molecules we want to allow to be passed to the second channel, or shut out the complete possibility of one isotope travelling to the narrower channel, therefore achieving isotopic separation.

We also avoid the general assumption that only ground states would be occupied by the molecules. As the calculations show, we have considered a series of energy levels. It is true that the probability of higher order energy levels being occupied are pretty remote at low temperatures. However, our discussion includes a wide range of temperature, and at sufficiently high ones, these energy levels are indeed accessible. As our calculation shows, if the second nanochannel has effective radius of 0.6 nm or 0.3 nm, then no hydrogen molecules are allowed to pass whereas a certain percentage of deuterium molecules are allowed. This in turn creates a situation where the second channel contains pure deuterium, free of hydrogen.

TABLE 4.6: First few energy levels of hydrogen (in K) inside second nanotube for varying tube radii (m is fixed at 0)

E_n	a=0.9	a=0.8	a=0.7	a=0.6	a=0.5	a=0.4	a=0.3	a=0.2	a=0.1
E_0	-199.141	-198.913	-198.520	-198.067	-197.217	-195.651	-192.269	-182.606	-130.424
E_1	-195.474	-194.272	-192.518	-189.817	-185.336	-177.088	-159.267	-108.352	
E_2	-188.877	-185.923	-181.613	-174.974	-163.962	-143.691	-99.895		
E_3	-179.349	-173.863	-165.862	-153.534	-133.090	-95.453	-14.138		
E_4	-166.888	-158.093	-145.264	-125.499	-92.718	-32.372			
E_5	-151.496	-138.612	-119.820	-90.867	-42.848				
E_6	-133.172	-115.421	-89.530	-49.638					
E_7	-110.916	-88.520	-54.393	-1.813					

TABLE 4.7: First few energy levels of deuterium(in K) inside second nanotube for varying tube radii (m is fixed at 0)

E_n	a=0.9	a=0.8	a=0.7	a=0.6	a=0.5	a=0.4	a=0.3	a=0.2	a=0.1
E_0	-199.570	-199.456	-199.289	-199.032	-198.607	-197.823	-196.129	-191.291	-165.165
E_1	-197.734	-197.132	-196.254	-194.902	-192.658	-188.524	-179.606	-154.114	-16.457
E_2	-194.431	-192.952	-190.794	-187.470	-181.957	-171.807	-149.880	-87.230	
E_3	-189.660	-186.914	-182.908	-176.736	-166.500	-147.656	-106.944		
E_4	-183.422	-179.018	-172.595	-162.699	-146.287	-116.073	-50.797		
E_5	-175.715	-169.265	-159.856	-145.360	-121.318	-77.060			
E_6	-166.541	-157.654	-144.691	-124.718	-91.593	-30.615			
E_7	-155.899	-144.185	-127.098	-100.773	-57.113				

From the tables 4.6 and 4.7, it is clear that the energy levels rise as we make the radius of the second channel narrower. Now, following eq(3.8), we hypothesise that the molecules travelling into the second channel from the first channel are only those with appropriate energies(i.e energies corresponding to those in the narrower channel). Simply put, we take δE in eqn(3.8) to be 1 K and hence in reduced form the equation looks like

$$|E_2 - E_1| \leq 1 \quad (4.1)$$

where E_2 and E_1 are the energies in the second and first nanotube respectively. In other words, only molecules in the second channel whose energies are approximate subsets of those in the first channel are allowed, the others are constrained to remain in the first channel itself and not go beyond.

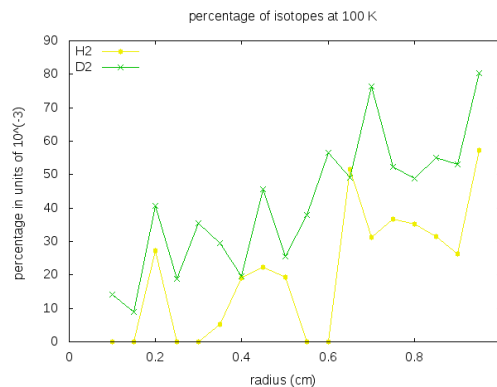


FIGURE 4.2: comparison between percentages at 100K

This drastically reduces the percentage of molecules that can travel into the second channel as very few energy levels in two channels are co-incident. One unexpected fact that is worth noticing is that when the radius of the narrower channel is 0.2 nm, all its computed energy levels are subsets (within a tolerance of 1K) of those of the wider channel (with radius of 1 nm). This observation is unique only in this case and does not apply for any other channel width that we investigated. This happens because the zeroes of Bessel function almost co-incide in such a situation. Another point to note is that more coincidences are possible only at lower temperatures (i.e at low energy levels) because the higher energy levels are only accessible at increased temperatures and these values are extremely unrealistic to be achieved physically.

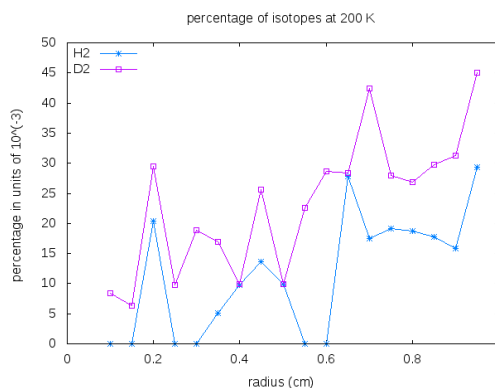


FIGURE 4.3: comparison between percentages at 200K

The figures above show extremely irregular behaviour and it is very hard to make sense of the results in a predictive kind of way. As shown in the figures above, there are multiple points in the range of 0.1-0.9 nm where hydrogen is totally cut-off from entering the second nanotube. However, these points are completely random though one can safely concur that if the second radii is close to the first one (larger than 0.7 nm in our case), then there is very little chance of perfect sieving under

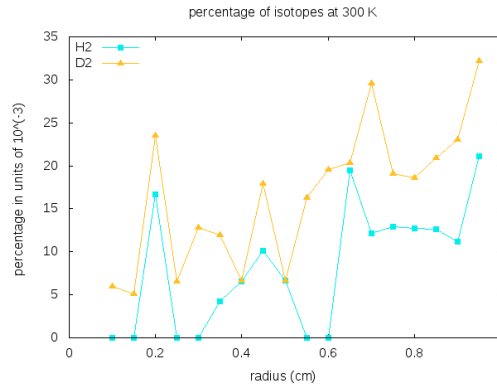


FIGURE 4.4: comparison between percentages at 300K

any condition. Another important point to note is that the deeper the potential well is, the better are the chances of sieving. This is because a deeper potential well allows for larger number of energy levels, and larger percentage of molecules to go through (provided the levels are approximately co-incident). A choice of a larger tolerance i.e $\Delta\tilde{E}'$, also allows for a higher number of co-incident energy levels.

4.4 A general theorem on correspondence

In the following section, we obtain a rule for coincidence of energy levels. In accordance with the above treatment, we propose a theorem for the special case when $a=1$ nm and b is varied.

Theorem: As $n, l \rightarrow \infty$, $b = \frac{n\pi}{l\pi} = \frac{n}{l}$ where n, l are integers.

Proof: The separation between zeroes of consecutive Bessel function approach π asymptotically. So, if we are looking for correspondences between zeroes of Bessel functions, we should have

$$b\lambda_l = a\lambda_n$$

or

$$b\lambda_l = \lambda_n$$

.

Here $\lambda_n = n\pi + c_n$ and $\lambda_l = l\pi + c_l$.

c_l, c_n are corrections because of the fact that the zeroes don't exactly coincide with multiples of π to begin with.

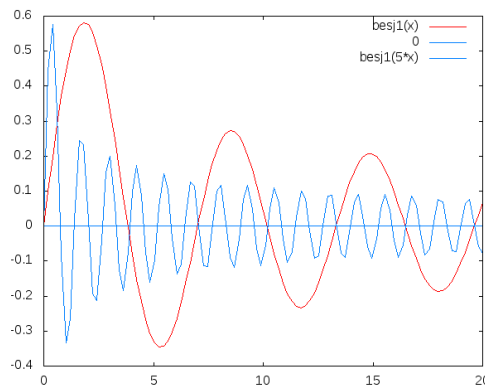


FIGURE 4.5: coincidence of zeroes of bessel function when $a=5b$

Now,

$$b(l\pi + c_l) = (n\pi + c_n) \implies b = \frac{n\pi}{l\pi + c_l} + \frac{c_n}{l\pi + c_l}$$

.

Since $l\pi \gg c_l$ as $l \rightarrow \infty$, the second term on R.H.S $\rightarrow 0$

Hence,

$$b = \frac{n\pi}{l\pi + c_l} \approx \frac{n\pi}{l\pi} = \frac{n}{l}$$

(proved)

However, this result is misleading if one is looking for coincidences with error smaller than δE . Also a point to note is that the coincidences are asymptotic, hence extremely unphysical in a real situation.

4.5 Comparison between percentage of H_2 and D_2 in the second channel

As we know, the molecules inside the channel have infinitely many quantized energy levels. However, for all practical purposes, these energy levels have a cut off which is dictated by the nature of the Maxwell-Boltzmann curve. More specifically, we ignore those energies which lie in the tail end of the distribution as the probability of molecules with these energies are small when compared to the bulk. The table below gives a cut off for the energies at various temperatures.

TABLE 4.8: Cutoff for Maxwell-Boltzmann distribution at various temperatures

temperature(K)	cutoff-energy(K)
77	400
100	600
200	1200
300	1500

In table 4.8, we give an approximation of the percentage of molecules (in units of 10^{-3}) for both species that are allowed into the second channel for various tube radii and varying temperature. The calculations are accomplished by first calculating the energy levels via eq(3.7) and then integrating eq(3.4) between the limits $E + \delta E$ to $E - \delta E$ to finally achieve the required percentage of molecules that are allowed inside the channel. ($\delta E/k_b$ is taken 1 K)

TABLE 4.9: Percentage of molecules (in units of 10^{-3}) allowed into the second channel

temp(K)	molecule	radius(nm)								
		0.9	0.8	0.7	0.6	0.5	0.4	0.3	0.2	0.1
77	H_2	31.73	44.11	38.26	0	20.05	25.55	0	31.25	0
	D_2	64.88	60.29	94.67	72.03	25.51	25.24	44.63	45.61	16.52
100	H_2	26.34	35.27	31.29	0	19.45	19.15	0	27.24	0
	D_2	52.95	48.89	76.30	56.46	19.72	19.57	35.55	40.76	14.12
200	H_2	15.66	18.72	17.54	0	9.86	9.78	0	20.32	0
	D_2	31.29	26.90	42.37	28.67	9.93	9.89	18.84	29.44	8.40
300	H_2	11.23	12.75	12.19	0	6.61	6.57	0	16.72	0
	D_2	23.04	18.57	29.60	19.59	6.64	6.62	12.81	23.56	5.94

As is evident from the table, deuterium in general has greater probability of passing into the second channel as compared to hydrogen. Also, specific tube radii allow almost no hydrogen (at least negligible compared to percentage of deuterium) to enter the second channel. This indicates that at these radii we have an almost perfect sieve for isotopes.

4.6 Distribution of nanotubes

Let us consider the situation where the nanotubes of varying radius are distributed randomly in a porous membrane and the gas molecules, which are inside a reservoir, are equally likely to access any one of them. We want to calculate the average percentage of molecules that are allowed to pass in such case. The average percentage of molecule absorbed is given by

$$\langle P \rangle = \int_{-\infty}^{\infty} P(\omega) f(\omega) d\omega$$

where $f(\omega)$ is the distribution function for the nanotubes.

Before we proceed with the calculation, in the table is given the actual percentage of molecules absorbed (in units of 10^{-3}) inside nanotubes with widths varying from 0.1 nm to 1 nm at room temperature.

We first consider the simple case of uniform distribution where $f(\omega)=1$. In this case, the formula for average percentage reduces to

$$\langle P \rangle = \int_{-\infty}^{\infty} P(\omega)f(\omega)d\omega \approx \int_0^1 P(\omega)f(\omega)d\omega = \sum_{i=0}^1 P_i(\omega)d\omega$$

Here $P_i(\omega)$ corresponds to $P_{0.1}(\omega), P_{0.2}(\omega)$ etc and $d\omega$ is the increment in width of the nanotubes which we have taken to be $0.1nm$. In this case the average percentage for H_2 and D_2 are given by $\langle P_{H_2} \rangle = 49.45 \times 10^{-3}$ and $\langle P_{D_2} \rangle = 70.69 \times 10^{-3}$ respectively.

Next we consider the case of gaussian distribution where $f(\omega) = \frac{1}{\sqrt{2\pi}\sigma} e^{-\frac{(\omega-\mu)^2}{2\sigma^2}}$ where μ =mean of the distribution and σ =the standard deviation of the distribution. The choice of mean and s.d in this case depends entirely on our discretion. However, it is evident that the distribution is limited between 0.1 and 1. We also know that about 99.7 percent of the total distribution lie within the range $\mu \pm 3\sigma$. Armed with this knowledge, we choose μ as 0.55 and σ as 0.15. Proceeding with the calculations, the respective percentages for H_2 and D_2 are given as $\langle P_{H_2} \rangle = 19.27 \times 10^{-3}$ and $\langle P_{D_2} \rangle = 27.59 \times 10^{-3}$.

We further try to refine our calculations by reducing $d\omega$ to $0.05 nm$. In the following table, the percentage of molecules absorbed for the new nanotubes are given.

TABLE 4.10: Percentage of molecules (in units of 10^{-3}) absorbed inside nanotubes with varying width at room temperature with $d\omega = 1$

temp(K)	molecule	radius(nm)									
		1.0	0.9	0.8	0.7	0.6	0.5	0.4	0.3	0.2	0.1
300	H_2	88.24	82.78	73.45	63.82	54.60	45.24	35.26	26.45	17.04	7.61
	D_2	125.05	117.53	104.35	91.27	77.57	64.61	52.08	38.10	24.81	11.52

With these modifications, we calculate the percentage for uniform distribution and find $\langle P_{H_2} \rangle = 46.98 \times 10^{-3}$, $\langle P_{D_2} \rangle = 67.27 \times 10^{-3}$.

For gaussian distribution, the same are given as $\langle P_{H_2} \rangle = 18.62 \times 10^{-3}$ and $\langle P_{D_2} \rangle = 26.79 \times 10^{-3}$ respectively.

4.6.1 Distribution of nanotubes in the second channel

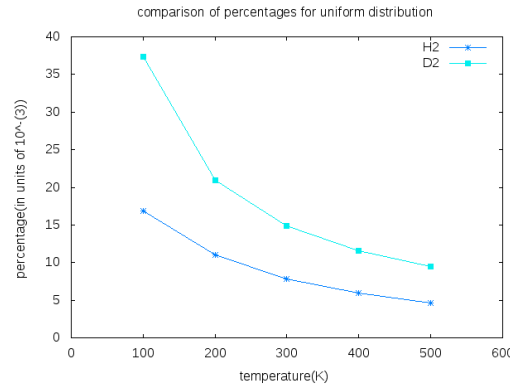


FIGURE 4.6: comparison of percentages of isotopes present inside the first nanotube for uniform distribution

Let us consider the situation where the nanotubes of varying radius are distributed randomly and the gas molecules, which are inside a reservoir, are equally likely to access any one of them. We want to calculate the average percentage of molecules that are allowed to pass in such case. This means that we have an ensemble of $1nm$ tubes to which tubes of radii varying from $0.95 nm$ to $0.1 nm$ are connected following a distribution. We want to calculate the average percentage of molecules

TABLE 4.11: Percentage of molecules (in units of 10^{-3}) absorbed inside nanotubes with varying width at room temperature with $d\omega = 1$

temp(K)	molecule	radius(nm)								
		0.95	0.85	0.75	0.65	0.55	0.45	0.35	0.25	0.15
300	H_2	85.14	78.67	67.89	59.01	48.88	40.13	30.85	21.52	13.01
	D_2	120.34	110.16	98.51	84.79	71.03	58.35	45.67	31.45	18.14

absorbed into the second channel under such conditions. The average percentage of molecule absorbed is given by

$$\langle P \rangle = \int_{-\infty}^{\infty} P(\omega) f(\omega) d\omega$$

where $f(\omega)$ is the distribution function for the nanotubes.

To do this bit, we first calculate the individual energy levels associated with each radius. Then we try to look for correspondences between the energy levels of different radii (by allowing a tolerance of $E/k_b=1 \text{ nm}$). For example, suppose an energy level for radius a is given as $E_1/k_b=-100.56 \text{ K}$ and that for radius b is given by $E_2/k_b=-99.87 \text{ K}$. These two energy levels are then considered to correspond because $1/k_b|E_1 - E_2| < 1 \text{ K}$.

The percentages are then calculated and integrating between the limits $E + \delta E$ to $E - \delta E$ to finally achieve the required percentage of molecules that are allowed inside the channel. ($\delta E/k_b$ is taken 1 K)

We first consider the simple case of uniform distribution where $f(\omega)=1$. In this case, the formula for average percentage reduces to

$$\langle P \rangle = \int_{-\infty}^{\infty} P(\omega) f(\omega) d\omega \approx \int_0^1 P(\omega) f(\omega) d\omega = \sum_{i=0}^1 P_i(\omega) d\omega$$

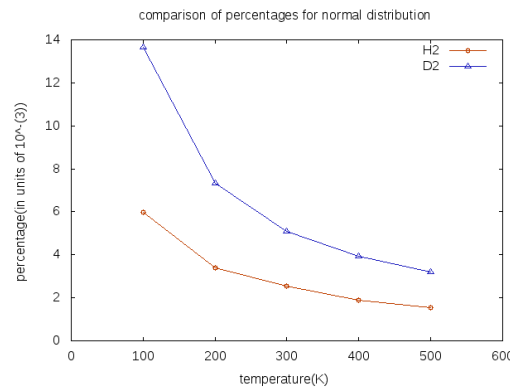


FIGURE 4.7: comparison of percentages of isotopes present inside the second nanotube for normal distribution

Here $P_i(\omega)$ corresponds to $P_{0,1}(\omega), P_{0,2}(\omega)$ etc and $d\omega$ is the increment in width of the nanotubes which we have taken to be 0.05 nm. In the following table, a comparison between the average percentage of hydrogen and deuterium molecules absorbed are given for different temperatures.

TABLE 4.12: Percentage of molecules (in units of 10^{-3}) absorbed inside nanotubes with varying temperatures considering uniform distribution

temp(K)	$\langle P_{H_2} \rangle$	$\langle P_{D_2} \rangle$
100	16.87	37.39
200	11.06	20.91
300	7.79	14.84

Next we consider the case of gaussian distribution where $f(\omega) = \frac{1}{\sqrt{2\pi}\sigma} e^{-\frac{(\omega-\mu)^2}{2\sigma^2}}$ where μ =mean of the distribution and σ =the standard deviation of the distribution. The choice of mean and s.d in this case depends entirely on our discretion. However, it is evident that the distribution is limited between 0.1 and 0.95. We also know that about 99.7 percent of the total distribution lie within the range $\mu \pm 3\sigma$. Armed with this knowledge, we choose μ as 0.50 and σ as 0.15.

TABLE 4.13: Percentage of molecules (in units of 10^{-3}) absorbed inside nanotubes with varying temperatures considering gaussian distribution

temp(K)	$\langle P_{H_2} \rangle$	$\langle P_{D_2} \rangle$
100	5.99	13.65
200	3.41	7.32
300	2.53	5.11

An important thing to note here is that the percentages increase when the temperature is decreased, while the reverse happens if temperature increases. This is due to the fact that most correspondences occur within the ground state and the first few excited states. As the temperature is increased, the occupation of

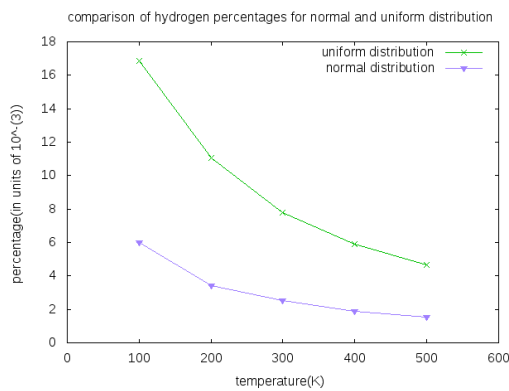


FIGURE 4.8: comparison of percentage of hydrogen inside second nanotube for different distributions

these states decrease as the molecules are encouraged to occupy higher order states.

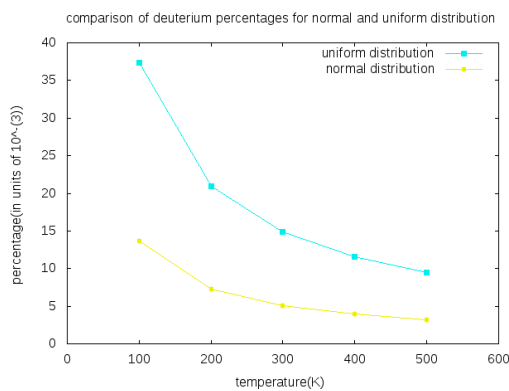


FIGURE 4.9: comparison of percentage of deuterium inside second nanotube for different distributions

Chapter 5

KINETIC SIEVING OF ISOTOPES

This section is devoted to the development and discussions related to the kinetic sieving of hydrogen and deuterium that were performed by us via MD simulation techniques. A major part of this work has been done in collaboration with Prof. Debra Bernhardt and Dr. Stefano Bernardi of AIBN, University of Queensland and in essence is somewhat similar to that performed by Kumar and Bhatia[14].

5.1 Theoretical Outline

We wished to study the kinetic sieving effect of hydrogen and deuterium through nanotubes using molecular dynamics (MD) simulation with the Feynman-Hibbs (FH) modified interaction potential

$$U_{FH}(r) = \left(\frac{6\mu}{\pi\beta\hbar^2}\right)^{\frac{3}{2}} \int d\mathbf{R} U(|\mathbf{R} + \mathbf{r}|) \exp(-6\mu R^2/\beta\hbar^2) \quad (5.1)$$

which is based on the variational treatment of the path integral. Ring Polymer Molecular Dynamics [21–24] was used for this variational treatment in our case.

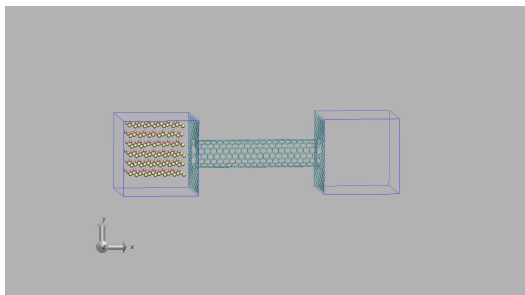


FIGURE 5.1: A physical representation of the simulation setup

Our MD simulations for hydrogen isotopes in carbon nanotube model the fluid-fluid and fluid-solid interactions according to Lennard-Jones (12-6) potential. For H_2 - H_2 and D_2 - D_2 interactions, the parameters used were $\epsilon_f/k_b=36.7$ K and $\sigma_f=0.2958$ nm whereas for the C - C interactions, the parameters were $\epsilon_s/k_b=37.26$ K and $\sigma_s=0.34$ nm. The fluid-solid interaction potential parameters were determined according to the Berthelot mixing rule. The model consists of a nanotube connected to two reservoirs at either ends. The first reservoir holds a combination of isotopes, and is thermostated via a Nosé-Hoover Thermostat. After an initial period of equilibration, the molecules are allowed to travel from one reservoir to the other one via the nanotube. A typical run consists of the same number of particles in the initial reservoir to begin with (indicating a molar concentration of 0.5 each) and after a certain time interval the molar concentration in the final chamber is calculated. The selectivity of deuterium over hydrogen is given by the ratio of molar concentrations in the initial and final reservoir and is defined as

$$S = \left(\frac{D_f}{D_i} \right) / \left(\frac{H_f}{H_i} \right) \quad (5.2)$$

where D_f and D_i respectively indicate the molar concentrations of deuterium in the final and initial reservoir (similarly for hydrogen). A selectivity value of greater than 1 indicates a preferential passage of deuterium into the final reservoir as compared to hydrogen.

In determining effective potential considering quantum effects, eq (5.1) is replaced by

$$U_{FH}(r) = U(r) + \frac{\beta\hbar^2}{24\mu} \left(U''(r) + 2\frac{U'}{r} \right) + \frac{\beta^2\hbar^4}{1152\mu^2} \left(15\frac{U'(r)}{r^3} + 4\frac{U'''(r)}{r} + U''''(r) \right) \quad (5.3)$$

which is obtained upon expanding the integrand in (5.1) upto R^4 . This same potential was used for both fluid-solid as well as solid-solid interactions. Such an approximation reduces computation time, and also overcomes the singularity in the integrand at zero interparticle separation. Our simulations were run for 4 nanotubes of different radii viz. (2,8), (6,6), (8,8) and (10,10) within a temperature range of 20-100 K. Multiple runs were made to account for statistical error.

5.2 Results

We expected that the selectivity values would be greater than 1 in general, indicating more deuterium to accumulate in the final reservoir as compared to hydrogen. This happens because of the steric hindrance caused due to the increase in effective size of the solid-fluid interactions.

For the lighter hydrogen, the quantum effects are stronger compared to the heavier deuterium, and as such the former faces a much higher hindrance. This results in an easier passage of deuterium through the nanotube. Considering Bertholet's

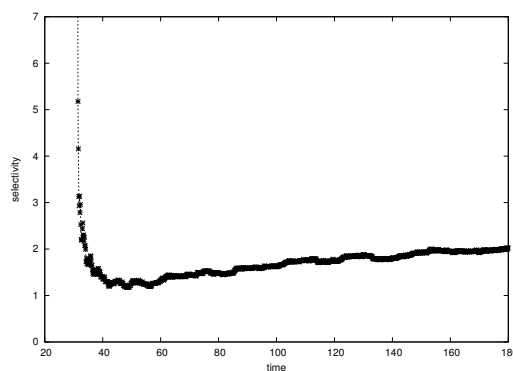


FIGURE 5.2: sample run of a single simulation (this one is for a (6,6) nanotube at 40 K)

mixing rule, the effective fluid solid interaction parameters are given as $\epsilon_{fs}=36.93$ K and $\sigma_{fs}= 0.317$ nm. So, any nanotube with radii smaller than 0.317 nm is not expected to allow any molecule to pass through. Sure enough, when we ran the simulations for (8,0) and (3,6) nanotubes (with radii 0.309 nm and 0.307 nm respectively), we didn't get any molecule to go through to the final chamber, confirming the theoretical prediction.

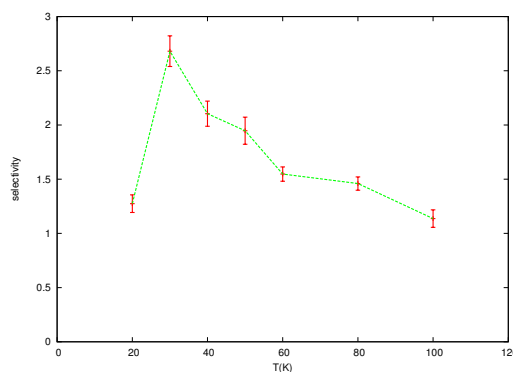


FIGURE 5.3: selectivity vs T curve for a (2,8) nanotube

Fig 5.2 shows the variation of selectivity of a with simulation time for sample run. The discontinuity at the beginning corresponds to the equilibration period. The initial values of selectivity are also pretty high due to the fact that only a few

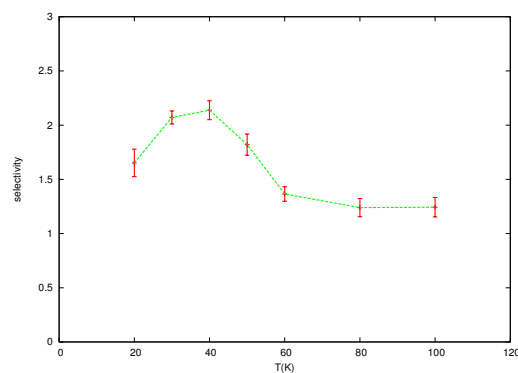


FIGURE 5.4: selectivity vs T curve for a (6,6) nanotube

number of molecules are allowed to go inside. However, as time grows, more and more particles go in through the nanotube into the final chamber, giving a much better estimation of selectivity. Also after certain period of time, the selectivity values reach a stable value, indicating that a sort of optimization has been established inside the nanotube whereby no more molecules can pass through on account of high pressure inside.

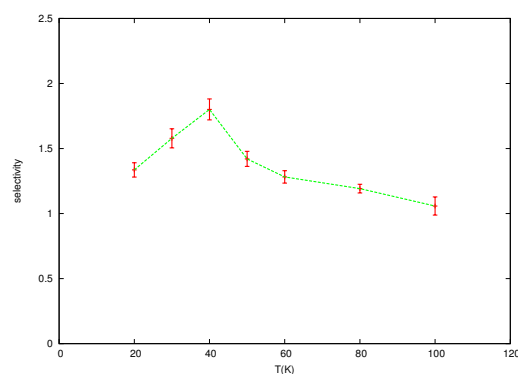


FIGURE 5.5: selectivity vs T curve for an (8,8) nanotube

Fig 5.3 shows the variation of selectivity with temperature for a (2,8) nanotube. The graph peaks at 30 K, with a mean value of 2.681 before tapering off as the temperature is increased. A similar kind of behaviour is shown for (6,6) and (8,8) nanotubes (fig 5.4 and fig 5.5 respectively), with the peak shifting to 40 K and with peak mean values of 2.138 and 1.801 respectively. However, the (10,10) tube

deviates from this standard behaviour (fig 5.6), showing a peak value of 1.449 at 20K before decreasing monotonically with increasing temperature. This can be attributed to the fact that the quantum effects already start to wane in (10,10) tube (with a radius of 0.678 nm) and hence display an almost classical behaviour.

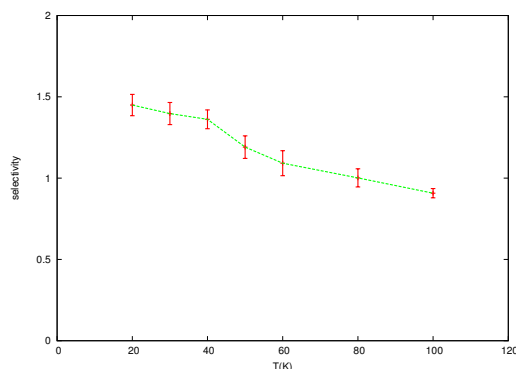


FIGURE 5.6: selectivity vs T curve for a (10,10) nanotube

The selectivity values that we obtained via kinetic sieving are noticeably much less in magnitude than those obtained via equilibrium sieving done in previous works. As a matter of fact, Kumar and Bhatia[14] have obtained much higher values (selectivity of 21.7 at 65K) via a similar procedure but using zeolite rho. However, the low values are not surprising considering the fact that the sieving in our case is not achieved by means of a pore, but the molecules have to travel through the entire length of the tube to be sieved. The crowding effect inside the tube due to the accumulation of molecules can severely affect selectivity.

Fig 5.7 shows how the molar concentration for the two isotopes vary inside the initial and the final reservoir. It is interesting to note that for the first reservoir, both the isotopes start initially with the same molar concentration. However, as simulation time progresses, the molar concentration of H_2 decreases while that of D_2 decreases. This indicates that as time goes by, more and more D_2 molecules are

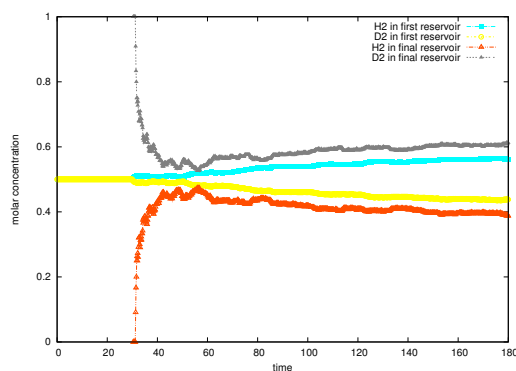


FIGURE 5.7: change in molar concentration of the isotopes inside the two reservoirs for a typical simulation (this one is for a (6,6) nanotube at 40K)

prone to leave the initial reservoir as compared to their lighter counterpart. This difference of concentration in the first chamber is compensated by an increased D_2 concentration in the final reservoir when compared to a depleted H_2 number, indicating that D_2 molecules are more probable to travel to the final reservoir via the nanotube, resulting in an effective selectivity greater than 1.

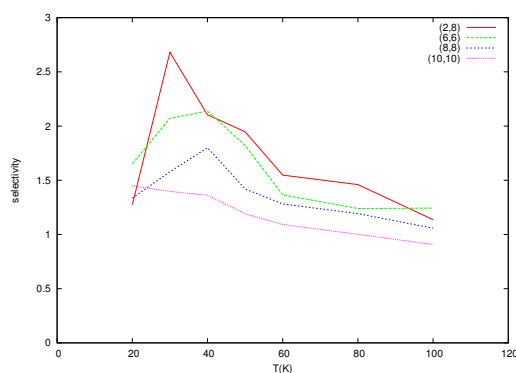


FIGURE 5.8: comparison of selectivity for different nanotubes

However, despite the quantitative difference, the qualitative behaviour of the selectivity-temperature curve in our case shows remarkable similarity with that obtained by Kumar and Bhatia, with a distinct peak obtained at 65 K for them (30 K and 40 K for us), before decreasing. The difference in temperature at which the peak value is observed can be conveniently attributed due to the difference of sieving material used in both cases (zeolite rho vs carbon nanotube). Also it is

important to note that the two smallest tubes (2,8) and (6,6) show the highest selectivity.

Chapter 6

CONCLUSION

We have, in our works, thus tried to achieve sieving through nanotubes by means of equilibrium as well as kinetic sieving. In case of the former, we have seen that a combination of two nanotubes can actually act as a perfect sieve under certain conditions, with a selectivity of deuterium over hydrogen being infinite. Another advantage of the approach we adopted was that sieving could be carried over a wide temperature range as the quantum energy levels are independent of temperature. So even at moderately high temperatures, a perfect sieving can be observed. Though the analytical calculations were done considering a square well potential and under ideal circumstances, more realistic nanotube potentials are also expected to show similar kind of behaviour, albeit with less efficiency. A two nanotube sieving device can thus be made to work like a perfect sieve. It should also be interesting to observe how roughness of the nanotube walls (varying radius) affect sieving. A two nanotube system can be a perfect precursor for such kind of study. As far as kinetic sieving is considered, the selectivity values we obtained are much lower than those obtained in previous works, suggesting a not so attractive proposition of its use as a sieving device at first glance. However, we feel that this kind of setup is much more realistic and is open to further explorations. Nevertheless, a two nanotube system for this kind of setup can also be studied

and the results compared with the single nanotube case. Since the molecules show a kind of ballistic transport through the nanotubes, it is very difficult to calculate the traditional transport properties such as diffusivity in the case of kinetic sieving we have considered. But the ballistic transport properties in such a case can also be an interesting aspect to ponder upon in the future.

Bibliography

- [1] J.J.M Beenakker, V.D Borman, and S.Yu.Krylov. (molecular transport in subnanometer pores:zero point energy, reduced dimensionality and quantum sieving). *Chemical Physics Letters*, 232:379–382, January 1995.
- [2] Qinyu Wang, Sivakumar R.Challa, David S.Sholl, and J.Karl Johnson. (quantum sieving in carbon nanotubes and zeolites). *Physical Review Letters*, 82(5):956–958, February 1999.
- [3] Sivakumar R.Challa, David S.Sholl, and J.Karl Johnson. (light isotope separation in carbon nanotubes through quantum molecular sieving). *Physical Review B*, 63(245419):1–9, August 2001.
- [4] George Stan and Milton W.Cole. (low coverage adsorption in cylindrical pores). *Surface Science*, 395:280–291, January 1998.
- [5] George Stan, Vincent H. Crespi, Milton W. Cole, and Massimo Boninsegni. (interstitial he and ne in nanotube bundles). *Journal of Low Temperature Physics*, 113(3-4):447–452, November 1998.
- [6] Noriaki Hamada, Shin ichi Sawada, and Atsushi Oshiyama. (new one-dimensional conductors: Graphitic microtubules). *Physical Review Letters*, 68(10):1579–1581, March 1992.

-
- [7] A.D. Crowell and J.S. Brown. (laterally averaged interaction potentials for 1h₂ and 2h₂ on the (0001) graphite surface). *Surface Science*, 123(2-3):296–304, December 1982.
- [8] B. C. Hathorn, B. G. Sumpter, and D. W. Noid. (contribution of restricted rotors to quantum sieving of hydrogen isotopes). *Physical Review A*, 64(022903): 1–7, July 2001.
- [9] Tun Lu, Stephen K. Gray, and Evelyn M. Goldfield. (quantum states of molecular hydrogen and its isotopes in single-walled carbon nanotubes). *Journal of Physical chemistry B*, 107(107):12989–12995, October 2003.
- [10] R. A. Trasca, M. K. Kostov, and M. W. Cole. (isotopic and spin selectivity of h₂ adsorbed in bundles of carbon nanotubes). *Physical Review B*, 67(035410): 1–8, January 2003.
- [11] Tun Lu, Evelyn M. Goldfield, and Stephen K. Gray. (quantum states of hydrogen and its isotopes confined in single-walled carbon nanotubes:dependence on interaction potential and extreme twodimensional confinement). *Journal of Physical chemistry B*, 110(3):1742–1751, January 2006.
- [12] Taner Yildirim and A. B. Harris. (quantum dynamics of a hydrogen molecule confined in a cylindrical potential). *Physical Review B*, 67(245413):1–15, June 2003.
- [13] Giovanni Garberoglio, Michael M. DeKlavon, and J. Karl Johnson. (quantum sieving in single-walled carbon nanotubes: effect of interaction potential and rotationaltranslational coupling). *Journal of Physical chemistry B*, 110(4): 17331741, January 2006.
- [14] A. V. Anil Kumar and Suresh K. Bhatia. (quantum effect induced reverse kinetic molecular sieving in microporous materials). *Physical Review Letters*, 95(245901):1–4, December 2005.

-
- [15] A. V. Anil Kumar, Herve Jobic, and Suresh K. Bhatia. (quantum effect induced reverse kinetic molecular sieving in microporous materials). *Journal of Physical chemistry B*, 110:16666–166671, August 2006.
- [16] Xuebo Zhao, Silvia Villar-Rodil, Ashleigh J. Fletcher, and K. Mark Thomas. (kinetic isotope effect for h₂ and d₂ quantum molecular sieving in adsorption/desorption on porous carbon materials). *Journal of Physical chemistry B*, 110:9947–9955, May 2006.
- [17] Marlies Hankel, Hong Zhang, Thanh X. Nguyen, Suresh K. Bhatia, Stephen K. Gray, and Sean C. Smith. (kinetic modelling of molecular hydrogen transport in microporous carbon materials). *Physical Chemistry Chemical Physics*, 13(17):7834–7844, March 2011.
- [18] Stephanie Reich, Christian Thomsen, and Janina Maultzsch. *Carbon nanotubes: Basic concepts and physical properties*. Wiley-VCH, 2004.
- [19] R.W Robinett. (visualizing solutions for the circular infinite well in quantum and classical mechanics). *American Journal of Physics*, 64(4):440–445, April 1996.
- [20] George B. Arfken and Hans J. Webber. *Mathematical Methods for Physicists*. Elsevier, 2005.
- [21] Ian R. Craig and David E. Manolopoulos. (quantum statistics and classical mechanics: Real time correlation functions from ring polymer molecular dynamics). *Journal of Chemical Physics*, 121(8):3368–3373, 2004.
- [22] Bastiaan J. Braams and David E. Manolopoulos. (quantum statistics and classical mechanics: Real time correlation functions from ring polymer molecular dynamics). *Journal of Chemical Physics*, 125(12):124105–12413, 2006.

-
- [23] Thomas E. Markland and David E. Manolopoulos. (an efficient ring polymer contraction scheme for imaginary time path integral simulations). *Journal of Chemical Physics*, 129(2):024105–024114, 2008.
- [24] Thomas E. Markland and David E. Manolopoulos. (a refined ring polymer contraction scheme for systems with electrostatic interactions). *Chemical Physics Letters*, 464(4-6):256–261, October 2008.